Journal of Intelligent and Robotic Systems **15**: 67–133, 1996.

Robust Sliding-mode Control Applied to a 5-Link Biped Robot

SPYROS TZAFESTAS[1], MARK RAIBERT[2] and COSTAS TZAFESTAS[1]
[1]*Intelligent Robotics and Control Unit, National Technical University of Athens, Zografou 15773, Athens, Greece and*
[2]*Artificial Intelligence Laboratory, MIT, 545 Technology Square, Cambridge, MA, 02139, U.S.A.*

(Received in final form: 13 September 1993)

Abstract. In this paper the application of robust control to a 5-link biped robotic model is investigated through the sliding mode approach, and compared to pure computed torque control. The biped consists of five links, namely the torso and two links in each leg. These links are connected via four (two hip and two knee) rotating joints which are considered to be friction-free and driven by independent d.c. motors. The locomotion of the biped is assumed to be constrained on the sagittal plane. The paper provides a full derivation of the biped dynamic model (single-leg support phase, biped-in-the-air phase) and an outline of the computed torque and sliding mode control algorithms. The simulation results were derived with two sets of parameters (one of which corresponds to a human-sized biped) and several degrees of parametric uncertainty (from 10% to 200%). In all cases the results obtained through the sliding mode control were much better than those obtained with the computed torque control. This superiority was shown to become stronger as the degree of uncertainty and the size of the biped increases.

Key words. Biped robots, robust control, sliding mode control, single leg-support phase, computer torque control.

1. Introduction

The area of legged robotic systems has attracted throughout the years the attention of a large number of researchers and is now at a sufficiently mature state [1]. Bipeds are a class of legged robots that attempt to imitate the human-type locomotion. The first and simplest model used for the study of some of the characteristics of human walking is the inverted pendulum [2–4]. More complex models with more degrees of freedom were used mainly after 1980 for a more complete study of human walking as well as for the actual construction of biped robotic systems [5–11]. For example, Miura and Shinoyama [7] have used a 3-link model (torso and two simple legs) to construct a biped robot (BIPER-3) the behavior of which was studied on both the sagittal and frontal planes. Furusho and Masubuchi [8, 9] have used a planar 5-link model as a basis for the construction of their initial biped (Kenkyaku-1) which was later improved by

adding two more links (Kenkyaku-2, weight 40 kg, height 1.10 m) [10]. A very interesting anthropomorphic biped robot (called BLR-G1) was constructed by Sano and Furusho [11]. An improved 9-link version of it (BLR-G2) has a weight of 25-kg and a height of 0.97 m. An important work was also carried out in Waseda University (Tokyo) where a series of bipeds have been constructed (since 1973) [13]. The most recent of them (WasedaLeg-12) is weighted 107 kg and has 1.80 m height. This robot is equiped with modern force sensors on its feet and joints, and uses hydraulic actuators. The minimum step time realised by WL-12 was 1.3 sec and the maximum stride 0.30 m.

Our purpose in the present paper is to investigate the effectiveness of sliding mode control when applied to such biped robots. As a first step in this study, we selected a 5-link model (i.e. no ankle joints and feet). The results are encouraging and suggest the use of sliding mode control in actual experimental and other bipeds. Since the derivation of the Euler–Lagrange model of 5-link bipeds is not readily available we provide here the full procedure, including the equations of the impact of the free leg on the ground. The control algorithms are well known and readily available in the robotics literature and so only a short outline of them is provided here. The approach used for the sliding mode control is the one presented by Slotine [14–16]. For the convenience of the reader the basic steps of Slotine's derivation are repeated here too. The simulation results were obtained for a small-sized biped and for a human-sized biped in order to explore the effectiveness of control under a large repertory of situations. The parametric uncertainty considered ranges from 10% to 200% and both the walking-on-an-horizontal-plane-surface mode and the staircase-climbing mode were studied. In all cases the sliding mode performs much better with the superiority of its performance being stregthened as the degree of uncertainty increases.

2. The 5-Link Biped Robotic Model

In this section the dynamic equations of the 5-link biped robot of concern will be derived in the two distinct phases of 'single-leg support' and 'biped-in-the-air'. As a preparation for this, the kinematic model of the biped will be first presented.

2.1. KINEMATICS MODEL

The biped robot under study has the form shown in Figure 1 [9]. It consists of five links, namely the torso (link 3) and two links in each leg (the upper legs, i.e. links 2 and 4, and the lower legs, i.e. links 1 and 5). These links are connected via four rotating joints; two hip joints and two knee joints, which are considered to be friction free and each one is driven by an independent DC motor. It is assumed that the locomotion of this biped mechanism is constrained on the sagittal plane as shown in Figure 1. Since this biped does not possess ankle joints and feet it is not possible to increase or reduce its speed using the torques

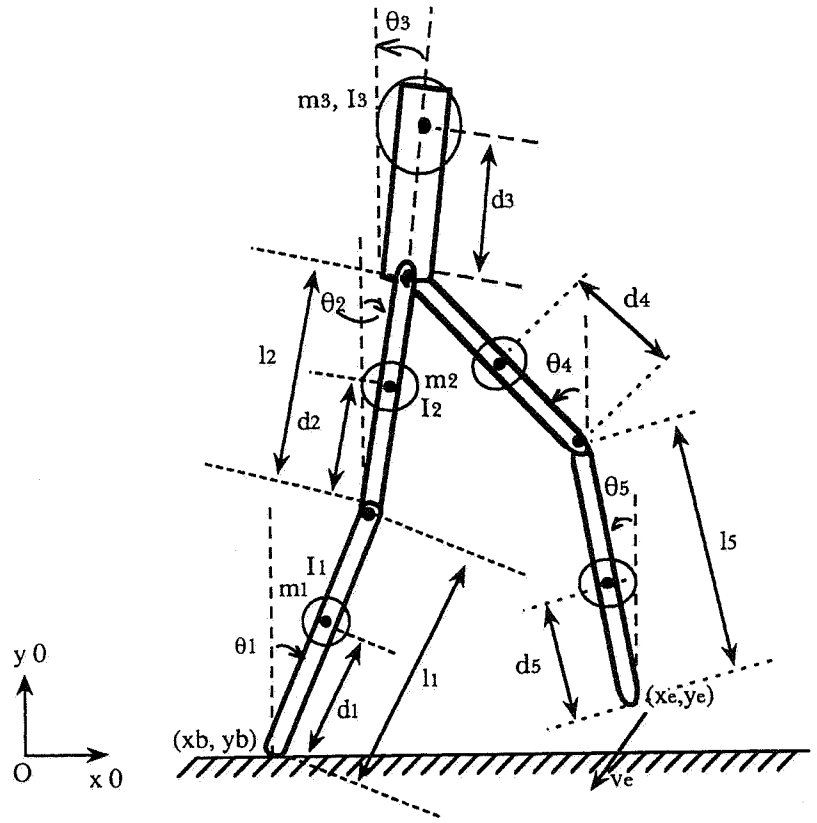

Fig. 1. 5-link planar biped robot model.

in these joints. However, a biped can walk without direct control of its angular momentum through the ankle torque, but indirectly through appropriate use of the effect of gravity.

The parameters shown in Figure 1 are as follows:

m_i: mass of link i.
l_i: length of link i.
d_i: distance between the mass center of link i and its lower joint.
I_i: moment of inertia with respect to an axis passing through the mass center of link i and being perpendicular to the motion plane.
θ_i: angle of link i with respect to the vertical (the positive direction of θ_i, $i = 1, 2, 3, 4, 5$, is the one shown in the figure).
O_0-$x_0y_0z_0$: the fixed coordinate frame (i.e. the inertia reference system).
(x_b, y_b): position of the point of support.

(x_e, y_e): position of the free end.
$\underline{v}_e$: velocity of the free end.

From Figure 1 it follows that

$$x_e = x_b + l_1 \sin\theta_1 + l_2 \sin\theta_2 + l_4 \sin\theta_4 + l_5 \sin\theta_5, \tag{1a}$$
$$y_e = y_b + l_1 \cos\theta_1 + l_2 \cos\theta_2 - l_4 \cos\theta_4 - l_5 \cos\theta_5 \tag{1b}$$

and

$$\underline{v}_e = \begin{pmatrix} \dot{x}_e \\ \dot{y}_e \end{pmatrix} = \begin{pmatrix} l_1 \cos\theta_1 \\ -l_1 \sin\theta_1 \end{pmatrix} \dot{\theta}_1 + \begin{pmatrix} l_2 \cos\theta_2 \\ -l_2 \sin\theta_2 \end{pmatrix} \dot{\theta}_2 + \begin{pmatrix} l_4 \cos\theta_4 \\ l_4 \sin\theta_4 \end{pmatrix} \dot{\theta}_4 + \begin{pmatrix} l_5 \cos\theta_5 \\ l_5 \sin\theta_5 \end{pmatrix} \dot{\theta}_5. \tag{2}$$

Now if $(cgx,\ cgy)$ are the coordinates of the biped's center of mass, and $(x_{ci},\ y_{ci})$ the coordinates of the center of mass of link i, then

$$\left.\begin{aligned} x_{c1} &= d_1 \sin\theta_1, \\ y_{c1} &= d_1 \cos\theta_1, \\ x_{c2} &= l_1 \sin\theta_1 + d_2 \sin\theta_2, \\ y_{c2} &= l_1 \cos\theta_1 + d_2 \cos\theta_2, \\ x_{c3} &= l_1 \sin\theta_1 + l_2 \sin\theta_2 + d_3 \sin\theta_3, \\ y_{c3} &= l_1 \cos\theta_1 + l_2 \cos\theta_2 + d_3 \cos\theta_3, \\ x_{c4} &= l_1 \sin\theta_1 + l_2 \sin\theta_2 + (l_4 - d_4) \sin\theta_4, \\ y_{c4} &= l_1 \cos\theta_1 + l_2 \cos\theta_2 - (l_4 - d_4) \cos\theta_4, \\ x_{c5} &= l_1 \sin\theta_1 + l_2 \sin\theta_2 + l_4 \sin\theta_4 + (l_5 - d_5) \sin\theta_5, \\ y_{c5} &= l_1 \cos\theta_1 + l_2 \cos\theta_2 - l_4 \cos\theta_4 - (l_5 - d_5) \cos\theta_5 \end{aligned}\right\} \tag{3}$$

and

$$\left.\begin{aligned} cgx &= \frac{(m_1 x_{c1} + m_2 x_{c2} + m_3 x_{c3} + m_4 x_{c4} + m_5 x_{c5})}{(m_1 + m_2 + m_3 + m_4 + m_5)}, \\ cgy &= \frac{(m_1 y_{c1} + m_2 y_{c2} + m_3 y_{c3} + m_4 y_{c4} + m_5 y_{c5})}{(m_1 + m_2 + m_3 + m_4 + m_5)}. \end{aligned}\right\} \tag{4}$$

2.2. DYNAMIC MODEL: SINGLE-LEG-SUPPORT PHASE

This situation is schematically shown in Figure 2. It is assumed that the friction of the ground is sufficiently large to ensure no slipping of the supporting end.

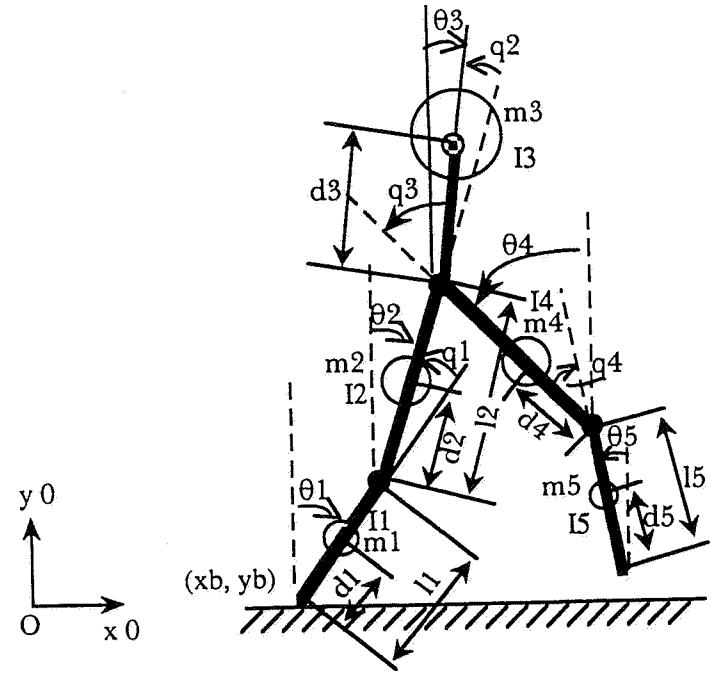

Fig. 2. Biped with one leg in the air.

Since the motion of the biped is performed on the plane of Figure 1 the angles θ_i $(i = 1, 2, \ldots, 5)$ are sufficient for fully describing its configuration.

The Lagrange dynamic model describing the motion of the biped in this phase is found to be (see Appendix 1 for the derivation):

$$\underline{D}(\underline{\theta}) \cdot \ddot{\underline{\theta}} + \underline{h}(\underline{\theta}, \dot{\underline{\theta}}) + \underline{G}(\underline{\theta}) = \underline{T}_\theta, \tag{5}$$

where

$$\left.\begin{aligned} \underline{\theta} &= [\theta_1, \theta_2, \ldots, \theta_5]^T, \\ \underline{T}_\theta &= [T_{\theta 1}, T_{\theta 2}, \ldots, T_{\theta 5}]^T, \\ \underline{h}(\underline{\theta}, \dot{\underline{\theta}}) &= \operatorname{col}\left[\sum_{j=1(j\neq i)}^{5} \left(h_{ijj}(\dot{\theta}_j)^2\right)\right], \\ \underline{G}(\underline{\theta}) &= \operatorname{col}[G_i(\underline{\theta})], \\ \underline{D}(\underline{\theta}) &= [D_{ij}(\underline{\theta})], \qquad i, j = 1, 2, \ldots, 5. \end{aligned}\right\} \tag{6}$$

Here, $T_{\theta i}$ is the generalized torque that corresponds to θ_i, col $[a_i]$ is a column vector with elements a_i, and $\underline{D}(\underline{\theta})$ is the inertia matrix of the biped with elements:

$$\underline{D} = [D_{ij}], \qquad i,j = 1,\ldots,5, \tag{7}$$

$$\begin{aligned}
&D_{11} = I_1 + m_1 d_1^2 + (m_2 + m_3 + m_4 + m_5) l_1^2,\\
&D_{12} = p_{12}\cos(\theta_1 - \theta_2), \qquad p_{12} = m_2 d_2 l_1 + (m_3 + m_4 + m_5) l_1 l_2,\\
&D_{13} = p_{13}\cos(\theta_1 - \theta_3), \qquad p_{13} = m_3 l_1 d_3,\\
&D_{14} = p_{14}\cos(\theta_1 + \theta_4), \qquad p_{14} = m_4 l_1 (l_4 - d_4) + m_5 l_1 l_4,\\
&D_{15} = p_{15}\cos(\theta_1 + \theta_5), \qquad p_{15} = m_5 l_1 (l_5 - d_5),\\
&D_{21} = D_{12},\\
&D_{22} = I_2 + m_2 d_2^2 + (m_3 + m_4 + m_5) l_2^2,\\
&D_{23} = p_{23}\cos(\theta_2 - \theta_3), \qquad p_{23} = m_3 l_2 d_3,\\
&D_{24} = p_{24}\cos(\theta_2 + \theta_4), \qquad p_{24} = m_4 l_2 (l_4 - d_4) + m_5 l_2 l_4,\\
&D_{25} = p_{25}\cos(\theta_2 + \theta_5), \qquad p_{25} = m_5 l_2 (l_5 - d_5),\\
&D_{31} = D_{13}, \qquad D_{32} = D_{23},\\
&D_{33} = I_3 + m_3 d_3^2, \qquad D_{34} = D_{35} = 0,\\
&D_{41} = D_{14}, \qquad D_{42} = D_{24}, \qquad D_{43} = D_{34} = 0,\\
&D_{44} = I_4 + m_4 (l_4 - d_4)^2 + m_5 l_4^2,\\
&D_{45} = p_{45}\cos(\theta_4 - \theta_5), \qquad p_{45} = m_5 l_4 (l_5 - d_5),\\
&D_{51} = D_{15}, \qquad D_{52} = D_{25}, \qquad D_{53} = D_{35} = 0, \qquad D_{54} = D_{45},\\
&D_{55} = I_5 + m_5 (l_5 - d_5)^2,
\end{aligned}$$

The elements h_{ijj} and G_i are as follows:

$$\begin{aligned}
&h_{122} = p_{12}\cdot\sin(\theta_1 - \theta_2), \qquad h_{133} = p_{13}\cdot\sin(\theta_1 - \theta_3),\\
&h_{144} = -p_{14}\cdot\sin(\theta_1 + \theta_4), \qquad h_{155} = -p_{15}\cdot\sin(\theta_1 + \theta_4),\\
&h_{211} = -p_{12}\cdot\sin(\theta_1 - \theta_2), \qquad h_{233} = p_{23}\cdot\sin(\theta_2 - \theta_3),\\
&h_{244} = -p_{24}\cdot\sin(\theta_2 + \theta_4), \qquad h_{255} = -p_{25}\cdot\sin(\theta_2 + \theta_5),\\
&h_{311} = -p_{13}\cdot\sin(\theta_1 - \theta_3), \qquad h_{322} = -p_{23}\cdot\sin(\theta_2 - \theta_3),\\
&h_{344} = h_{355} = 0,
\end{aligned}$$

$$\begin{aligned}
&h_{411} = -p_{14}\cdot\sin(\theta_1 + \theta_4), \qquad h_{422} = -p_{24}\cdot\sin(\theta_2 + \theta_4),\\
&h_{433} = 0, \qquad h_{455} = p_{45}\cdot\sin(\theta_4 - \theta_5),\\
&h_{511} = -p_{15}\cdot\sin(\theta_1 + \theta_5), \qquad h_{522} = -p_{25}\cdot\sin(\theta_2 + \theta_5),\\
&h_{533} = 0, \qquad h_{544} = -p_{45}\cdot\sin(\theta_4 - \theta_5),
\end{aligned} \tag{8}$$

$$\left.\begin{aligned}
G_1 &= -[m_1 d_1 + (m_2 + m_3 + m_4 + m_5) l_1] g \sin\theta_1,\\
G_2 &= -[m_2 d_2 + (m_3 + m_4 + m_5) l_2] g \sin\theta_2,\\
G_3 &= -[m_3 d_3] g \sin\theta_3,\\
G_4 &= [m_4 (l_4 - d_4) + m_5 l_4] g \sin\theta_4,\\
G_5 &= [m_5 (l_5 - d_5)] g \sin\theta_5.
\end{aligned}\right\} \tag{9}$$

Now, let $\underline{\tau} = [\tau_1, \tau_2, \tau_3, \tau_4]^T$ be the vector of the driving torques of the four joints of the biped, where (Figure 2):

$\tau 1$: driving torque of the knee of the supporting leg;

$\tau 2$: driving torque of the hip of the supporting leg;

$\tau 3$: driving torque of the hip of the free leg;

$\tau 4$: driving torque of the knee of the free leg.

If q_1, q_2, q_3 and q_4 are the relative angle deflections of the corresponding joints, then (see Figure 2):

$$q_1 = \theta_1 - \theta_2,\ q_2 = \theta_2 - \theta_3,\ q_3 = \theta_3 + \theta_4,\ q_4 = \theta_4 - \theta_5$$

and so the relation

$$T_{\theta i} = \sum_{j=1}^{4} \tau_j \frac{\partial q_j}{\partial \theta_i}, \qquad i = 1,2,\ldots,5,$$

gives:

$$T_\theta = E \cdot \underline{\tau}, \tag{10}$$

where E is the 5×4 matrix

$$E = \begin{bmatrix} 1 & 0 & 0 & 0\\ -1 & 1 & 0 & 0\\ 0 & -1 & 1 & 0\\ 0 & 0 & 1 & 1\\ 0 & 0 & 0 & -1 \end{bmatrix}.$$

Thus the biped dynamic model (5) becomes

$$\underline{D}(\underline{\theta}) \cdot \ddot{\underline{\theta}} + \underline{h}(\underline{\theta}, \dot{\underline{\theta}}) + \underline{G}(\underline{\theta}) = E \cdot \underline{\tau}. \tag{11}$$

We observe that only four of the five degrees of freedom $\theta_1, \theta_2, \ldots, \theta_5$ can be controlled directly by the four driving torques τ_1, τ_2, τ_3 and τ_4. The angle θ_1 at the contact point with the ground (hypothetical joint 0) is controlled only indirectly using the gravitational effect. The presence of this non (directly) controllable degree of freedom is one of the most important characteristics of the locomotion of our biped robot. A similar property characterizes the other legged locomotion mechanisms too.

To facilitate the control procedure, which is to be described in Section 3, the model (11) is transformed to (for the details see Appendix 2):

$$\underline{D}_q(\underline{q}) \cdot \ddot{\underline{q}} + \underline{h}_q(\underline{q}, \dot{\underline{q}}) + \underline{G}_q(\underline{q}) = \underline{T}_q, \tag{12a}$$

where (here $T_{q0} = 0$):

$$\underline{q} = \begin{bmatrix} q_0 \\ q_1 \\ \vdots \\ q_4 \end{bmatrix}, \quad \underline{h}_q = \begin{bmatrix} h_{q0} \\ h_{q1} \\ \vdots \\ h_{q4} \end{bmatrix}, \quad \underline{G}_q = \begin{bmatrix} G_{q0} \\ G_{q1} \\ \vdots \\ G_{q4} \end{bmatrix}, \quad \underline{T}_q = \begin{bmatrix} T_{q0} \\ T_{q1} \\ \vdots \\ T_{q4} \end{bmatrix}, \tag{12b}$$

and

$$\left.\begin{aligned} D_q(i,1) &= A_{i1} + A_{i2} + A_{i3} - A_{i4} - A_{i5}, \\ D_q(i,2) &= -A_{i2} - A_{i3} + A_{i4} + A_{i5}, \\ D_q(i,3) &= -A_{i3} + A_{i4} + A_{i5}, \\ D_q(i,4) &= A_{i4} + A_{i5}, \\ D_q(i,5) &= -A_{i5}, \end{aligned}\right\} (i = 1, \ldots, 5). \tag{12c}$$

This model uses the variables q_i $(i = 0, 1, \ldots, 4)$ instead of θ_i $(i = 1, 2, \ldots, 5)$, where q_0 corresponds to the hypothetical joint 0 at the contact point (x_b, y_b) with $q_0 = \theta_1$.

2.3. DYNAMIC MODEL: BIPED IN THE AIR

Suppose now that at the moment when the free leg touches the ground, the supporting leg leaves immediately the ground. This means that at the moment of collision of the free end with the ground the constraint $x_b = y_b =$ constant and $\dot{x}_b = \dot{y}_b = 0$, which was valid in the single-leg-support phase, is removed (see Figure 2). This implies that the dynamic model (5) or (12a) of the single-leg-support phase cannot be applied to compute the instantaneous changes of the

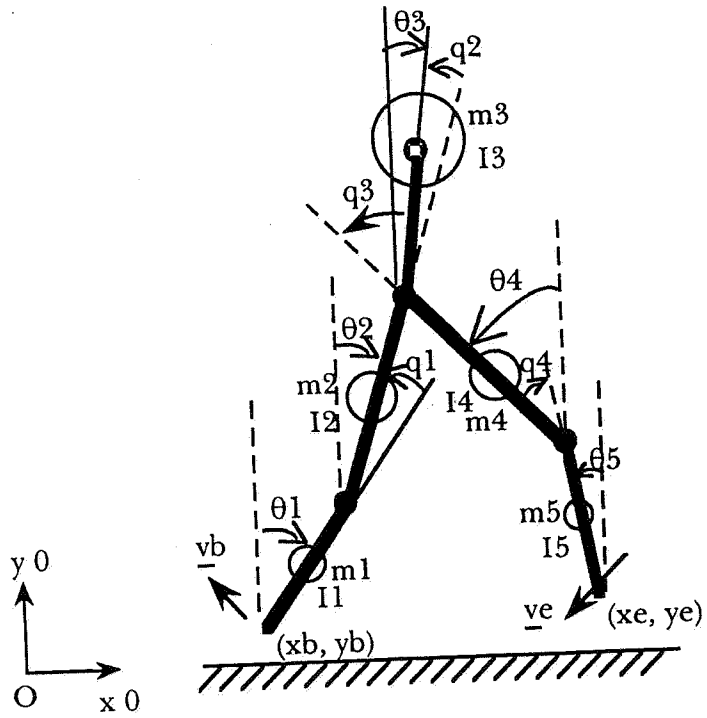

Fig. 3. Biped with both legs in the air.

joint angular velocities at the moment when the free end of the biped collides with the ground.

Our purpose here is to present the biped dynamic equations when both legs are in the air (Figure 3). In this case, for a full description of the configuration and the position of the biped, one needs, in addition to θ_i $(i = 1, 2, \ldots, 5)$ the coordinates x_b and y_b of the left end of the biped (Figure 3).

Applying the standard procedure through the Lagrange equations (see Appendix 3) one finds the following dynamic model for the biped in the air:

$$\underline{D}_a(\underline{\theta}_a) \cdot \ddot{\underline{\theta}}_a + \underline{h}_a(\underline{\theta}_a, \dot{\underline{\theta}}_a) + \underline{G}_a(\underline{\theta}_a) = \underline{T}_a, \tag{13}$$

where

$$\underline{\theta}_a = [\theta_1,\ \theta_2,\ \theta_3,\ \theta_4,\ \theta_5,\ x_b,\ y_b]^T,$$
$$\underline{G}_a = [Ga(1), \ldots, Ga(7)]T,$$
$$G_a(i) = G_i, \qquad i = 1, 2, \ldots, 5, \qquad G_a(6) = 0,$$

$$\underline{G}_a(7) = \left(\sum_{i=1}^{5} m_i\right) g = m_{\text{total}} \cdot g, \tag{14}$$

$$D_a(i,j) = D_{ij}, \qquad i = 1,\ldots,5, \quad j = 1,\ldots,5,$$

$$\left.\begin{aligned}
&D_a(1,6) = p_{16}\cos\theta_1, \qquad D_a(1,7) = -p_{17}\sin\theta_1,\\
&p_{16} = p_{17} = m_1 d_1 + (m_2 + m_3 + m_4 + m_5) l_1,\\
&D_a(2,6) = p_{26}\cos\theta_2, \qquad D_a(2,7) = -p_{27}\sin\theta_2,\\
&p_{26} = p_{27} = m_2 d_2 + (m_3 + m_4 + m_5) l_2,\\
&D_a(3,6) = p_{36}\cos\theta_3, \qquad D_a(3,7) = -p_{37}\sin\theta_3,\\
&p_{36} = p_{37} = m_3 d_3,\\
&D_a(4,6) = p_{46}\cos\theta_4, \qquad D_a(4,7) = p_{47}\sin\theta_4,\\
&p_{46} = p_{47} = m_4(l_4 - d_4) + m_5 l_4,\\
&D_a(5,6) = p_{56}\cos\theta_5, \qquad D_a(5,7) = p_{57}\sin\theta_5,\\
&p_{56} = p_{57} = m_5(l_5 - d_5),\\
&D_a(6,i) = D_a(i,6), \qquad i = 1,\ldots,5,\\
&D_a(6,6) = (m_1 + m_2 + m_3 + m_4 + m_5) = m_{\text{total}},\\
&D_a(6,7) = 0,\\
&D_a(7,i) = D_a(i,7), \qquad i = 1,\ldots,5,\\
&D_a(7,7) = (m_1 + m_2 + m_3 + m_4 + m_5) = m_{\text{total}}.
\end{aligned}\right\} \tag{15}$$

For the 7×1 vectors $\underline{T}_a$ and $\underline{h}_a$ we have

$$\left.\begin{aligned}
&T_a(i) = T_\theta(i), \qquad i = 1,\ldots,5,\\
&T_a(6) = T_{xb} = 0, \qquad T_a(7) = T_{yb} = 0,
\end{aligned}\right\} \tag{16}$$

$$\left.\begin{aligned}
&h_a(i) = h(i), \qquad i = 1,\ldots,5,\\
&h_a(6) = -p_{16}(\dot\theta_1)^2\sin\theta_1 - p_{26}(\dot\theta_2)^2\sin\theta_2 - p_{36}(\dot\theta_3)^2\sin\theta_3\\
&\qquad - p_{46}(\dot\theta_4)^2\sin\theta_4 - p_{56}(\dot\theta_5)^2\sin\theta_5,\\
&h_a(7) = -p_{17}(\dot\theta_1)^2\cos\theta_1 - p_{27}(\dot\theta_2)^2\cos\theta_2 - p_{37}(\dot\theta_3)^2\cos\theta_3\\
&\qquad + p_{47}(\dot\theta_4)^2\cos\theta_4 + p_{57}(\dot\theta_5)^2\cos\theta_5.
\end{aligned}\right\} \tag{17}$$

The elements D_{ij}, G_i, h_i and $T_{\theta i}$ are determined using Equations (7) through (10). The dynamic model (13)–(17) will be used in Section 2.4 for the computation

of the sharp changes in the angular velocities of the biped's links at the moment of changing the supporting leg, which happens when each step of the biped is completed.

2.4. IMPACT OF THE FREE END ON THE GROUND: INSTANTANEOUS EXCHANGE OF THE SUPPORTING LEG

As mentioned before when the free end of the biped, at the completion of each step, comes into contact with the ground, then an instantaneous exchange of the support of the biped to this end is taking place, while the other end (i.e. the previous supporting leg) leaves immediately the ground. This process is assumed to take place in an infinitesimal time interval, equal to the duration of the impact of the free end with the ground. The instantaneous change $\Delta\dot{\underline{\theta}}$ of the angular velocities $\dot\theta_i$, $i = 1,2,\ldots,5$, of the links, at the moment of the collision of the free end with the ground, is given by (for the derivation see Appendix 4) [17]:

$$\Delta\dot{\underline{\theta}} = \underline{D}_a^{-1} \cdot \underline{J}_a^T \cdot \left(\underline{J}_a \cdot \underline{D}_a^{-1} \cdot \underline{J}_a^T\right)^{-1} \cdot \Delta\dot{\underline{x}}_e, \tag{18}$$

where $\underline{D}_a$ is the inertia matrix (15) of the model (13). The new angular velocities of the links, after the exchange of the supporting leg, are used as initial conditions for the new step. In this way one can simulate and study the continuous locomotion of the biped.

The 2×7 Jacobian matrix J_a of the biped in the air is given by

$$\underline{J}_a = \frac{\partial \underline{x}_e}{\partial \underline{\theta}_a},$$

where the position vector $\underline{x}_e = [x_e,\ y_e]^T$ is given by (1), and $\underline{\theta}_a$ is the vector defined in (14). Using Equation (1a–b) one finds that:

$$\left.\begin{aligned}
&J_a(1,1) = l_1\cos\theta_1, \qquad J_a(2,1) = -l_1\sin\theta_1,\\
&J_a(1,2) = l_2\cos\theta_2, \qquad J_a(2,2) = -l_2\sin\theta_2,\\
&J_a(1,3) = 0, \qquad J_a(2,3) = 0,\\
&J_a(1,4) = l_4\cos\theta_4, \qquad J_a(2,4) = l_4\sin\theta_4,\\
&J_a(1,5) = l_5\cos\theta_5, \qquad J_a(2,5) = l_5\sin\theta_5,\\
&J_a(1,6) = 1, \qquad J_a(2,6) = 0,\\
&J_a(1,7) = 0, \qquad J_a(2,7) = 1.
\end{aligned}\right\} \tag{19}$$

Given that the velocity $\underline{v}_e$ becomes zero immediately after the collision with the ground, we have

$$\Delta\dot{\underline{x}}_e = -\dot{\underline{x}}_{e,\text{before}},$$

where $\dot{\underline{x}}_{e,\text{before}}$ is the velocity of the free end just before its contact with the ground. Therefore, the formula (18) gives

$$\dot{\underline{\theta}}_{\text{after}} = \dot{\underline{\theta}}_{\text{before}} + \underline{D}_a^{-1} \cdot \underline{J}_a^T \cdot \left(\underline{J}_a \cdot \underline{D}_a^{-1} \cdot \underline{J}_a^T\right)^{-1} \cdot \left(-\dot{\underline{x}}_{e,\text{before}}\right), \tag{20}$$

where $\dot{\underline{\theta}}_{\text{before}}$ and $\dot{\underline{\theta}}_{\text{after}}$ are the link velocities just before and just after the exchange of the supporting leg, respectively. It should be remarked here that the angular displacements of the joints do not change during the infinitesimal time interval of the collision, and so $\underline{D}_a$ and J_a in (18) or (20) are computed at the configuration of the biped at the moment of the collision.

3. Robust Control of the 5-Link Biped

As we have seen in Section 2, the dynamic performance of the biped is described by the model (12a) in the single-leg support phase, and by the model (13) when both legs are in the air. These models have exactly the same form, which for convenience is rewritten here as

$$\underline{D}(\underline{q}) \cdot \ddot{\underline{q}} + \underline{h}(\underline{q}, \dot{\underline{q}}) = \underline{\tau}, \tag{21}$$

where $\underline{\tau}$ is the vector of the driving forces and here the term $\underline{h}(\underline{q}, \dot{\underline{q}})$ involves all terms due to centripetal, Coriolis and gravitational forces. This term is strongly nonlinear and its effect increases drastically as the velocities of the biped's joints increase. Any linear control law ignores totally these nonlinearities, which actually couple the joints, with the result of reducing the accuracy of the trajectory tracking, especially at large operational velocities. The approach of linearizing the dynamic model (21) about some (fixed) operating point $\underline{x}_0 = [\underline{q}_0, \dot{\underline{q}}_0 = 0]$ and applying linear control laws is based on the assumption that the system state actually remains in the closed vicinity of $\underline{x}_0$. If this is not true (which is the case in most practical situations) then the performance of this approach may not be acceptable.

In addition to the existence of the nonlinearities, the system involves uncertainties due to several sources, the primary of which is the uncertainty in the biped robot parameters. This parametric uncertainty requires the introduction of suitable nonlinear terms in the control law that make it robust in the uncertainty.

Our purpose here is to study and compare the performance of the computed torque control (which is nonlinear) and the sliding mode control (which robustifies the computed torque control and makes it highly insensitive to parametric and other uncertainties), when applied to the biped locomotion described above.

3.1. BIPED COMPUTED TORQUE CONTROL

The computed torque control is actually based on the feedback linearization technique, i.e. on the use of a control law structure similar to that of the system's

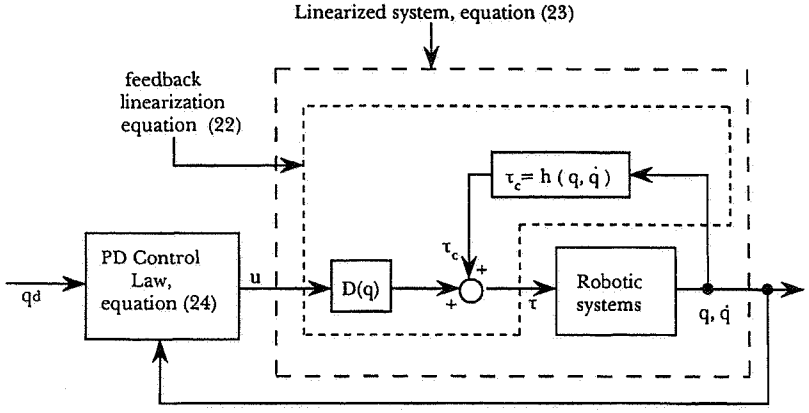

Fig. 4. Structure of computed torque-control.

dynamic model. Thus, the computed torque control law for the model (21) has the structure:

$$\underline{\tau} = \underline{D}(\underline{q})\underline{u} + \underline{h}(\underline{q}, \dot{\underline{q}}) \tag{22}$$

and eliminates the nonlinearities involved in the model (21).

Indeed, using the control law (22) in (21), and assuming that $\underline{D}(\underline{q})$ is invertible (away from the singular configurations), yields:

$$\ddot{\underline{q}} = \underline{u}. \tag{23}$$

The model (23) represents a set of $n = 5$ decoupled double integration systems, each one of which can be controlled by a suitable linear control law.

A useful decoupled control law is the proportional plus derivative control law, which has the form

$$\underline{u} = \ddot{\underline{q}}_d - \underline{K}_D \cdot \dot{\tilde{\underline{q}}} - \underline{K}_P \cdot \tilde{\underline{q}}, \tag{24}$$

where $\tilde{q}_j = q_j(t) - q_{dj}(t)$, $\underline{q}_d(t)$ is the desired joint trajectory vector and

$$\underline{K}_D = \text{diag}\left[K_{Dj}\right], \qquad \underline{K}_P = \text{diag}\left[K_{Pj}\right].$$

The block diagram of the resulting closed-loop computed-torque control system is as shown in Figure 4. The closed-loop equation for the error $\tilde{\underline{q}}(t)$ is

$$\ddot{\tilde{\underline{q}}} + K_D \cdot \dot{\tilde{\underline{q}}} + K_P \cdot \tilde{\underline{q}} = 0. \tag{25}$$

It is easy to verify that if the matrices $\underline{K}_D$ and $\underline{K}_P$ are positive definite (i.e. if $K_{Dj} > 0$ and $K_{Pj} > 0$ for all j) then the tracking error $\tilde{\underline{q}}(t)$ tends to zero

asymptotically as $t \to \infty$. If λ is the desired bandwidth (undamped cyclic natural frequency) then, for obtaining a critically damped closed-loop performance one must select

$$\underline{K}_D = \text{diag}\,[2\lambda] \qquad \text{and} \quad \underline{K}_P = \text{diag}\,[\lambda^2]. \tag{26}$$

The bandwidth λ should be selected sufficiently large in order to get a fast response, but it should not exceed a certain limit in order to avoid the excitation of possible unmodelled high frequency characteristics and to be compatible with the sampling rate used.

The biggest practical problem that arises is due to the time required to compute the quantities $\underline{D}(\underline{q})$ and $\underline{h}(\underline{q}, \dot{\underline{q}})$ and there exist many techniques to overcome this difficulty [18, 19]. A good solution is to use two different sampling periods: a large one for the computation of $\underline{D}(\underline{q})$ and $\underline{h}(\underline{q}, \dot{\underline{q}})$ and a small sampling period for the controller (which is then able to partially cover the errors of the computation of $\underline{D}(\underline{q})$ and $\underline{h}(\underline{q}, \dot{\underline{q}})$).

3.2. SLIDING MODE ROBUST CONTROL

The basic disadvantage of the computed torque control technique is that in practice $\underline{D}(\underline{q})$ and $\underline{h}(\underline{q}, \dot{\underline{q}})$ are not available exactly but approximately as $\widehat{\underline{D}}(\underline{q})$ and $\widehat{\underline{h}}(\underline{q}, \dot{\underline{q}})$. This uncertainty may be due to parametric uncertainty or to restricted computational power as indicated above or to both reasons. In practice therefore one can only use the control law (instead of (22)):

$$\underline{\tau} = \widehat{D}(\underline{q})\underline{u} + \widehat{\underline{h}}(\underline{q}, \dot{\underline{q}}) \tag{27a}$$

which leads to the system (instead of (23)):

$$\ddot{\underline{q}} = \left(D^{-1}\widehat{D}\right)\underline{u} + D^{-1}(\widehat{\underline{h}} - \underline{h}). \tag{27b}$$

This means that the system is actually coupled and nonlinear, and the linear control law (24) may lead to unacceptable performance. To face this problem many techniques are available which fall in two main categories namely *adaptive control techniques* and *robust control techniques*. Here, we have selected for application the sliding mode robust control technique which is easy to implement and leads to very good results.

The details of this technique can be found elsewhere [14–16]. Here we give only the basic equations of the algorithm.

Consider a system of the type

$$x^{(n)}(t) = a(\underline{x}) + b(\underline{x})u(t), \tag{28}$$

where $u(t)$ is the control input, $\underline{x} = [x, \dot{x}, \ldots, x^{(n-1)}]^T$ is the system's state vector, and the nonlinear functions $a(\underline{x})$ and $b(\underline{x})$ are not known exactly but with

errors $|\Delta a|$ and $|\Delta b|$ bounded by corresponding bounded continuous functions of $\underline{x}$. However, the sign of $b(\underline{x})$ is assumed to be known.

Let a time-varying surface $S(t)$ in the state space $\mathfrak{R}^n$ defined by the equation $s(\underline{x}, t) = 0$, where

$$s(\underline{x}, t) = \left(\frac{\mathrm{d}}{\mathrm{d}t} + \lambda\right)^{n-1} \cdot \tilde{x} \tag{29}$$

with λ being a positive constant that represents the control bandwidth. This surface is called the *sliding surface*.

Clearly, if $\underline{x}_d(t = 0) = \underline{x}(t = 0)$, where $\underline{x}_d(t)$ is the desired trajectory, the problem of making $\underline{x}(t) \equiv \underline{x}_d(t)$ is equivalent to that of making $s(x, t) = 0$ for all $t > 0$, i.e. to that of remaining on the sliding surface $S(t)$. Indeed, $s = 0$ represents a linear differential equation which, subject to the above initial conditions $\tilde{x}(0) = x(0) - x_d(0) = 0$, has the unique solution:

$$\underline{\tilde{x}} = \underline{x} - \underline{x}_d = \left[\tilde{x}, \dot{\tilde{x}}, \ldots, \tilde{x}^{(n-1)}\right]^T = 0.$$

Actually, constraining s within certain bounds corresponds to constraining the tracking vector $\tilde{x}$ in some interval. This means that s constitutes a convenient measure of the tracking accuracy.

Specifically, it can be shown that if $\tilde{x}(0) = 0$, then the condition

$$|s(t)| \leqslant \Phi \qquad \text{for all} \quad t \geqslant 0$$

implies the condition

$$|\tilde{x}^{(i)}(t)| \leqslant (2\lambda)^i \varepsilon \qquad \text{for all} \quad \varepsilon \geqslant 0 \quad \text{and} \quad t \geqslant 0 \tag{30}$$

for $i = 1, 2, \ldots, n-1$, where $\varepsilon = \Phi/\lambda^{n-1}$.

The problem of keeping the scalar function s to zero, can be solved if the control signal $u(t)$ in (28) is selected such that outside the surface $S(t)$ the following condition holds:

$$\frac{1}{2} \cdot \frac{\mathrm{d}}{\mathrm{d}t} s^2 \leqslant -\eta|s|, \tag{31}$$

where η is a positive constant.

The validity of the 'sliding condition' (31) ensures that the distance from the surface $s = 0$ (measured by s^2) decreases along all the trajectories of the system. Thus this condition forces all the trajectories of the system to slide on $S(t)$. This is why (31) is called *sliding condition*. Once a trajectory arrives at $S(t)$ it always remains on it, which means that $S(t)$ is an *invariant* region for the system.

The idea behind the use of (29) and (31) is to select an appropriate function of the tracking error and then to construct a feedback law u in (28) which

makes the function s^2 a Lyapunov function of the closed-loop system in spite the presence of the parametric uncertainties in $a(\underline{x})$ and $b(\underline{x})$. Moreover, the validity of the sliding condition (31) ensures that when $\underline{x}(t=0) \neq \underline{x}_d(t=0)$ [i.e. when $\underline{\tilde{x}}(t=0) \neq 0$], then the trajectories will slide to $S(t)$ in time less than $|s(t=0)|/\eta$. Once the trajectory reaches the sliding surface, the tracking error tends to zero asymptotically with a time constant $(n-1)/\lambda$.

On the basis of the above facts, the sliding controller design involves two steps. In the first a control law is selected for the system (28) such that the condition (31) is satisfied. To be able for this control law to face robustly the model inaccuracies, it should be discontinuous across the sliding surface $S(t)$. However, such a discontinuity leads to undesirable control chattering and must be suitably smoothened in such a way as to achieve an acceptable compromise between the trajectory tracking accuracy and the control bandwidth. These two steps are fully described in [16] and so here only the final results will be given. Thus, for a second-order system of the type (28) with $b(\underline{x}) \equiv 1$ and the function $a(\underline{x})$ being available only approximately as $\hat{a}(\underline{x})$ with error bound A:

$$|\hat{a} - a| \leqslant A \tag{32}$$

the best approximation $\hat{u}$ of a continuous control law that makes $\dot{s} = 0$, is

$$\hat{u} = -\hat{a} + \ddot{x}_d - \lambda \dot{\tilde{x}}, \tag{33}$$

where $\tilde{x} = x - x_d$ is the tracking error.

To satisfy the sliding condition (31): $\dot{s}s \leqslant -\eta|s|$ $(\eta > 0)$ in spite of the existence of the uncertainty in a, the term $k\text{sgn}(s)$ is added which is discontinuous on $s = 0$, i.e.

$$u = \hat{u} - k\,\text{sgn}(s), \qquad k = A + \eta, \tag{34a}$$

where

$$\text{sgn}(s) = \begin{cases} +1, & s > 0, \\ -1, & s < 0, \\ 0, & s = 0. \end{cases} \tag{34b}$$

A similar result can be obtained if we apply integral control, i.e. if we consider the integral $\int_0^t \tilde{x}(t')\mathrm{d}t'$ as the error variable of concern. The control law is again given by (34a–b) with

$$\hat{u} = -\hat{a} + \ddot{x}_d - 2\lambda\dot{\tilde{x}} - \lambda^2\tilde{x}. \tag{35}$$

If now $b(\underline{x}) \neq 1$ is known with uncertainty expressed by the bounds $b_{\min}$ and $b_{\max}$, i.e.

$$0 < b_{\min} \leqslant b \leqslant b_{\max} \tag{36}$$

then we choose as an estimator $\hat{b}(x)$ of $b(x)$ the geometric mean of $b_{\min}$ and $b_{\max}$, i.e.:

$$\hat{b} = \left(b_{\min} \cdot b_{\max}\right)^{1/2}. \tag{37}$$

Then using (37), the relation (36) can be written as

$$\beta^{-1} \leqslant \frac{\hat{b}}{b} \leqslant \beta, \qquad \beta = \left(\frac{b_{\max}}{b_{\min}}\right)^{1/2}, \tag{38}$$

where β is a kind of *gain margin*. Note that the uncertainty in the function $b(\underline{x})$ can be given either in the form (36) or directly in the form (38).

Now, the control law (34a) is replaced by

$$u = \hat{b}^{-1}(\hat{u} - k\,\text{sgn}(s)) \tag{39a}$$

with

$$k \geqslant \beta(A + \eta) + (\beta - 1)|\hat{u}|. \tag{39b}$$

Clearly, the increase in the amplitude k of the control discontinuity is needed in order to take into account the uncertainty in the gain b of the control signal.

To eliminate the 'chattering' of the control signal which is due to the discontinuity of u at $s = 0$, we smooth this discontinuity in a thin *boundary layer*:

$$B(t) = \{x, |s(x,t)| \leqslant \Phi\}, \qquad \Phi > 0, \tag{40}$$

around the discontinuity surface $s = 0$. Here Φ is the *thickness* of the boundary layer and $\varepsilon = \Phi/\lambda^{n-1}$ is its *width*. Outside $B(t)$ the control law is defined as in (34a) or (39a). The satisfaction of the sliding condition (31) now guarantees that the boundary layer $B(t)$ attracts all trajectories of the system. Thus, all trajectories that start inside $B(t=0)$ remain in $B(t)$ for all $t \geqslant 0$, whereas all those that start outside $B(t)$ slide towards it and enter it after some finite time.

Inside $B(t)$ we have

$$|s(t)| \leqslant \Phi \qquad \text{for all} \quad t \geqslant 0 \tag{41a}$$

which implies that

$$|\tilde{x}^{(i)}(t)| \leqslant (2\lambda)^i \varepsilon, \qquad i = 0, \ldots, n-1, \tag{41b}$$

where $\varepsilon = \Phi/\lambda^{n-1}$. This means that now we do not have a perfect trajectory tracking but an approximate tracking with accuracy determined by ε.

The smoothened control law for the case $b = \hat{b} = 1$ is {see (34a)}:

$$u = \hat{u} - \underline{k}(\underline{x})\text{sat}(s/\Phi), \tag{42a}$$

where sat(y) is the saturation function

$$\text{sat}(y) = \begin{cases} y, & |y| \leqslant 1, \\ \text{sgn}(y), & |y| > 1, \end{cases} \tag{42b}$$

and

$$\overline{k}(\underline{x}) = k(\underline{x}) - \dot{\boldsymbol{\Phi}}. \tag{42c}$$

The dynamic evolution of the thickness $\boldsymbol{\Phi}(t)$ of the boundary layer is governed by the equation

$$\dot{\boldsymbol{\Phi}} + \lambda \boldsymbol{\Phi} = k(\underline{x}_d) \tag{43}$$

which is obtained from (42c) by setting $\overline{k}(\underline{x}_d)/\boldsymbol{\Phi} = \lambda$.

Now, introducing (43) in (42c) gives

$$\overline{k}(\underline{x}) = k(\underline{x}) - k(\underline{x}_d) + \lambda \boldsymbol{\Phi} \tag{44}$$

which provides an alternative definition for $\overline{k}(\underline{x})$.

In the general case where $\widehat{b}/b \neq 1$ the above relations (43) and (44) are replaced by:

$$\dot{\boldsymbol{\Phi}} + \lambda \boldsymbol{\Phi} = \beta_d \cdot k(\underline{x}_d) \qquad \text{if} \quad k(\underline{x}_d) \geqslant \frac{\lambda \boldsymbol{\Phi}}{\beta_d}, \tag{45a}$$

$$\dot{\boldsymbol{\Phi}} + \frac{\lambda \boldsymbol{\Phi}}{\beta_d^2} = k(\underline{x}_d)/\beta_d \qquad \text{if} \quad k(\underline{x}_d) < \frac{\lambda \boldsymbol{\Phi}}{\beta_d} \tag{45b}$$

with initial condition $\boldsymbol{\Phi}(0) = \beta_d k(\underline{x}_d(0))/\lambda$, and

$$\overline{k}(\underline{x}) = k(\underline{x}) - k(\underline{x}_d) + \lambda \boldsymbol{\Phi}/\beta_d, \tag{46}$$

respectively, where $\beta_d = \beta(\underline{x}_d)$ {see (38)} and

$$\overline{k}(\underline{x}_d) = \lambda \boldsymbol{\Phi}/\beta_d. \tag{47}$$

Recalling that $\varepsilon = \boldsymbol{\Phi}/\lambda^{n-1}$ (see (41b)) the balancing Equation (47) implies that

$$\lambda^n \varepsilon \approx \beta_d \cdot k(\underline{x}_d), \tag{48}$$

i.e. the product of the nth power of the bandwidth λ and the maximum tracking error is approximately equal to the parameter uncertainty measured along the desired trajectory. The tradeoff Equation (48) tells us that the balancing conditions (43) and (45a, b) determine the best tracking performance that can be achieved with a given desired maximum control bandwidth and a given extent of parametric uncertainty. Of course, the desired trajectory $\underline{x}_d$ must also be sufficiently smooth for not exciting non-modelled high frequency components.

3.3. BIPED SLIDING MODE CONTROL

The above sliding mode robust control technique will now be applied to the 5-link biped robot model under study.

If $\widehat{D}$ and $\widehat{h}$ are the available estimates of D and h, at each time instant t, then the sliding controller has the form (27a) with u_i $(i = 1, 2, \ldots, n)$ being determined by

$$u_i = L_i(\underline{q})\left[\widehat{u}_i - \overline{k}_i(\underline{q}, \dot{\underline{q}})\text{sat}\left(s_i/\boldsymbol{\Phi}_i\right)\right], \tag{49}$$

where $\overline{k}_i(\underline{q}, \dot{\underline{q}})$ and $\boldsymbol{\Phi}_i$ $(i = 1, 2, \ldots, n)$ are defined by the balancing Equations (45a, b) and (46) and the $\widehat{u}_i$'s are chosen according to (35) as:

$$\widehat{u}_i = \ddot{q}_{di} - 2\lambda \dot{\widetilde{q}}_i - \lambda^2 \widetilde{q}_i, \tag{50}$$

where $\widetilde{q}_i = q_i - q_{di}$ is the tracking error of the trajectory of the ith joint. The sliding surfaces s_i in (49) are selected as:

$$s_i = \dot{\widetilde{q}}_i + 2\lambda \widetilde{q}_i + \lambda^2 \int_t \widetilde{q}_i(t')\mathrm{d}t', \tag{51}$$

where the indefinite integral $\int_t$ (which contains a constant to be determined) is defined so as $s_i(t = 0) = 0$. The gain coefficient $L_i(\underline{q})$ and the uncertainty bounds that are used for computing $\overline{k}_i(\underline{q}, \dot{\underline{q}})$ are discussed below.

Clearly, the main difference of the control law (49)–(50) from the simple computed torque PD control law is the presence of the robustification term $L_i(\underline{q}) \cdot \overline{k}_i(\underline{q}, \dot{\underline{q}})\text{sat}\,(s_i/\boldsymbol{\Phi}_i)$ which ensures stability and best performance in spite of the uncertainty in the biped model.

The amplitudes $\overline{k}_i(\underline{q}, \dot{\underline{q}})$ of the controller and the boundary layer thickness $\boldsymbol{\Phi}_i$ are computed from (45a, b) and (46) using the values of $\overline{k}_i(\underline{q}, \dot{\underline{q}})$ that result from known uncertainty bounds of $\underline{D}(\underline{q})$ and $\underline{h}(\underline{q}, \dot{\underline{q}})$.

To determine these bounds, let us define two vector sets $\underline{M}_j$ $(j = 1, 2, \ldots, n)$ and $\Delta \underline{D}_j$ $(j = 1, 2, \ldots, n)$ as

$$\underline{D}^{-1} = \left[\underline{M}_1\ \underline{M}_2 \cdots \underline{M}_n\right], \tag{52a}$$

$$\Delta \underline{D} = \widehat{\underline{D}} - \underline{D} = \left[\Delta \underline{D}_1\ \Delta \underline{D}_2 \cdots \Delta \underline{D}_n\right]. \tag{52b}$$

The vectors $\underline{M}_j$ and $\Delta \underline{D}_j$ depend only on the configuration of $\underline{q}$.

Introducing the control law (27a) into the biped model (21) gives the closed-loop equation

$$\ddot{\underline{q}} = (\underline{I} + \underline{D}^{-1}\Delta \underline{D})\underline{u} + \underline{D}^{-1}\Delta \underline{h}, \tag{53}$$

where $\underline{I}$ is the unit matrix and $\Delta\underline{h} = \hat{\underline{h}} - \underline{h}$.

It is now assumed that

$$\underline{M}_i^T \cdot \hat{\underline{D}}_i > 0, \qquad i = 1, \ldots, n. \tag{54}$$

This condition means that $\underline{D}^{-1}$ is symmetric and that u_i contributes to $\ddot{q}_i$ with a predictable sign. In practice, the condition (54) can be satisfied even for large parametric uncertainties, if $\hat{\underline{D}}$ is selected to be a positive definite diagonal matrix (involving for example the diagonal elements of the original matrix $\hat{\underline{D}}$).

The scalar bounds $\beta_i^{\min}$ and $\beta_i^{\max}$ (which may depend on $\underline{q}$) are then defined as

$$0 \leqslant \beta_i^{\min} \leqslant \underline{M}_i^T \cdot \hat{\underline{D}}_i \leqslant \beta_i^{\max}, \qquad i = 1, \ldots, n, \tag{55}$$

and the gains L_i of (49) are selected as {see (37)}:

$$L_i = \left(\beta_i^{\min}\beta_i^{\max}\right)^{-1/2}, \qquad i = 1, \ldots, n. \tag{56}$$

The corresponding gain margin β_i is equal to {see (38)}:

$$\beta_i = \left(\beta_i^{\max}/\beta_i^{\min}\right)^{1/2}, \qquad i = 1, \ldots, n. \tag{57}$$

Then the control discontinuity amplitudes $k_i(\underline{q}, \dot{\underline{q}})$ satisfy the conditions {see (39b)}:

$$k_i(\underline{q}, \dot{\underline{q}}) \geqslant \beta_i \Bigg[\left(1 - \beta_i^{-1}\right)|\hat{u}_i| + \left(\underline{M}_i^a\right)^T \Delta\underline{h}^a + \sum_{j \neq i} L_j \cdot |\ddot{q}_{dj}| \cdot \left|\underline{M}_i^T \hat{\underline{D}}_j\right| + \eta_i \Bigg] \tag{58}$$

for $i = 1, 2, \ldots, n$, where η_i are the positive constants that are used in the sliding conditions {see (31)} and $\underline{M}_i^a$, $\Delta\underline{h}^a$ denote the vectors with components the absolute values of the corresponding components of $\underline{M}_i$ and $\Delta\underline{h}$. In practice, an a priori worst-case analysis for the satisfaction of the conditions (55) and (58) is usually sufficient. In [16] it was shown that these conditions can be satisfied analytically if $n = 3$, i.e. in the case of a 6 degrees-of-freedom robot with decoupled the motion of the spherical end effector. In the general case a good approximation is obtained by computing the bounds (55) and (58) using, in place of the true $\underline{M}_i^a$, the estimates $\widehat{\underline{M}}_i^a$ which are obtained from the inversion of $\hat{\underline{D}}$. Similarly, the approximate upper bounds of $\Delta\underline{D}_i^a$ and $\Delta\underline{h}_i^a$ can be expressed in terms of $\hat{\underline{D}}_i^a$ and $\hat{\underline{h}}$. For example, if the only source of uncertainty in the estimate $\hat{\underline{D}}$ of the inertia matrix $\underline{D}$ is the fact that the moments of inertia are known with accuracy 10%, one can use the approximation $\Delta\underline{D}_i^a \leqslant (10\%)\hat{\underline{D}}_i^a$ where the inequality is meant component-wise. Thus, if the structure of the parametric uncertainty of the biped robot is known, the bounds (55) and (58) can be computed fairly easily.

4. Simulation Results

In this section the results of a simulation study will be presented for the case where the biped is walking on a planar horizontal surface and the case where the biped climbs a sequence of stairs of known height. The *computed torque* and *sliding mode* control laws will be applied and compared for various degrees of uncertainty. We shall see that a complete simplification of the system model as is done in the *local* (decoupled) proportional plus derivative (PD) control has very limited value. When the modelling errors and other uncertainties take large values (as in the case of a biped or an anthropomorphic robot) we have to use the full robotic model as is done in the computed torque-control technique. However, the computed-torque control requires an exact knowledge of the system parameters (inertia parameters, link lengths, etc.) which is not true in practice. This means that the control law is not *robust* as is the *sliding mode* control. These issues will be fully clarified and verified by the results that follow.

4.1. STEADY HORIZONTAL WALKING MODE

The 5-link biped robotic model shown in Figure 1 was used throughout the simulation study. Each of the four joints (two hip and two knee joints) are assumed to be driven by an independent motor. The motion of the biped is assumed to be constrained on the plane of the figure. The values of the parameters m_i, I_i, l_i, and d_i (see Section 2.1) are shown in Table I.

Our basic goal is to realize a steady stable gait on a horizontal plane. Such a gait can be obtained by feeding to the control system repeatedly at every-step the same reference signal [8]. In practice, the biped robot system should have a hierarchical structure, at the higher level of which the desired reference signal is selected (possibly using information about the surface of the ground from suitable sensors) (Figure 5). After the completion of each step, this reference signal is fed to the lower hierarchical level which involves the joint motion control system. The reference signal $q_r(t)$ for the steady walking on the horizontal plane is selected as described below. To keep the biped body in the vertical position (i.e. $\theta_3 = 0$, see Figure 1) we choose

$$q_{r2}(t) = \theta_2(t). \tag{59}$$

Table I. Parameters of the biped robot

Link	Mass m_i (kg)	Moment of inertia I_i (kg m)	Length l_i (m)	Location of center of mass d_i (m)
Torso	14.79	3.30×10^{-2}	0.486	0.282
Thigh	5.28	3.30×10^{-2}	0.302	0.236
Leg	2.23	3.30×10^{-2}	0.332	0.189

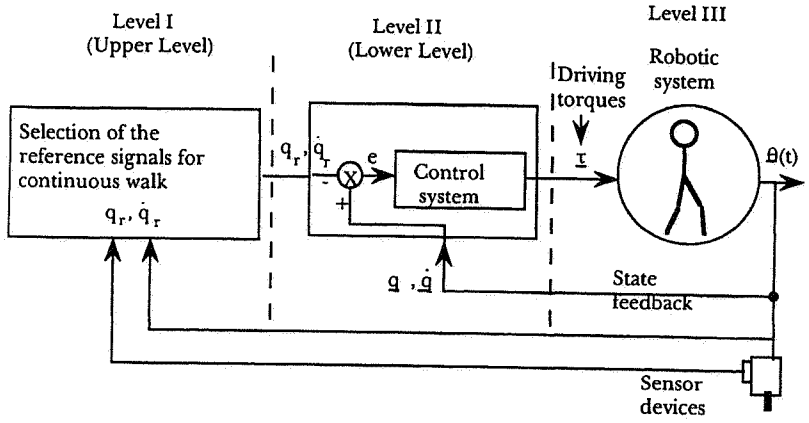

Fig. 5. Hierarchical structure of the robotic control system.

It is assumed that the transition of the supporting leg is instantaneous at the completion of each step. This assumption, which means that there is no phase of simultaneous support at both legs, is necessary since the biped has not 'soles' at the feet. Furthermore, because each foot has no ankle joint and sole, the reference signals must be selected so as to make use of the gravitational effect in order to increase the angular momentum of the biped about the supporting end toward the desired direction of motion. Thus the following gait model is considered which satisfies all the above requirements.

(i) At the moment where the free leg touches the surface of the ground, the supporting leg leaves immediately the ground.

(ii) The same reference signal $q_r(t)$ is fed repeatedly at each step.

(iii) Just before the contact of the free end with the ground, the reference signals $q_{r1}(t)$, $q_{r3}(t)$ and $q_{r4}(t)$ are given constant values q_{rs1}, q_{rs3} and q_{rs4}, respectively, as shown in Figure 6 which depicts the desired reference signals used for the control of joints 1, 3 and 4. In this way, the biped configuration at the moment where the free end touches the ground, is always the same, independently of the small deviation that may occur at the time where each step is completed. This leads to a constant step length (stride) over the whole duration of the biped walking. Let $q_{rs3} = q_h$ (say 30°) and $q_{rs1} = 0$. The reference signal q_{r4} in the knee joint is selected so as to keep this joint at the moment of contact of the free end with the ground at some nonzero value, in order to have a certain increase of the angular momentum upon the completion of the one leg support phase. For

example, let $q_{rs4} = q_k = q_h = 30° = 0.52$ rad as shown in Figure 7. Then from $q_{rs1} = 0$ it follows that $(l_1 + l_2)\cos q_{rs2} = l_4 \cos q_h + l_5$ and so

$$q_{rs2} = \arccos \frac{l_4 \cos q_h + l_5}{l_1 + l_2}. \tag{60}$$

$$\text{Stride} = (l_1 + l_2) \sin q_{rs2} + l_4 \sin q_h. \tag{61}$$

Thus the stride is kept constant throught.

(iv) Finally as is seen from Figure 7 the free leg (angle $q_{r3}(t)$) is moved forward very fast, such that the momentum increases in the correct direction because of the gravitational effect.

The reference signals described above were applied in all but the first (starting) step. At the starting step the slightly different reference signals of Figure 8 were used.

4.2. COMPUTED TORQUE VERSUS LOCAL PD CONTROL

Using the relative angle displacements as generalized variables the biped is described by the dynamic model (12a, b) where

$$\mathbf{T}_q = [0, \tau_1, \tau_2, \tau_3, \tau_4]^T \quad \text{and} \quad \mathbf{q} = [q_0, q_1, q_2, q_3, q_4]^T$$

($q_0 = \theta_1$ is the angle of rotation of the hypothetical joint 0 at the point of contact with the ground).

The computed torque control law has the form {see (22) and (12a, b)}:

$$\mathbf{T}_q = D_q(\mathbf{q})\mathbf{u} + \mathbf{h}_q + \mathbf{G}_q,$$

where $\mathbf{u}$ is the 5×1 state feedback vector with components

$$u_1 = -\frac{1}{D_q[1,1]} \cdot \left\{ \sum_{j=1}^{4} \left(D_q[1, j+1] \cdot u_{j+1} \right) + h_q(1) + G_q(1) \right\}, \tag{60a}$$

$$u_{j+1} = \ddot{q}_{rj} - K_{Dj}\dot{e}_j - K_{Pj}e_j, \qquad (j = 1,2,3,4). \tag{60b}$$

The component u_1 is selected such that $T_q(1) = 0$ which is required by the fact that the biped has the noncontrollable joint q_0. In (60b) q_{rj} $(j = 1,2,3,4)$ are the reference signals, $\ddot{q}_{rj}$ the desired acceleration of joint j at each time, and $e_j = q_j - q_{rj}$ the trajectory error. The constants K_{Dj} and K_{Pj} can be as described in Section 3.1, i.e. $K_{Dj} = 2\lambda$ and $K_{Pj} = \lambda^2$ $(i = 1,2,3,4)$ (see (26)). In this way a critically damped system is obtained with control bandwidth λ.

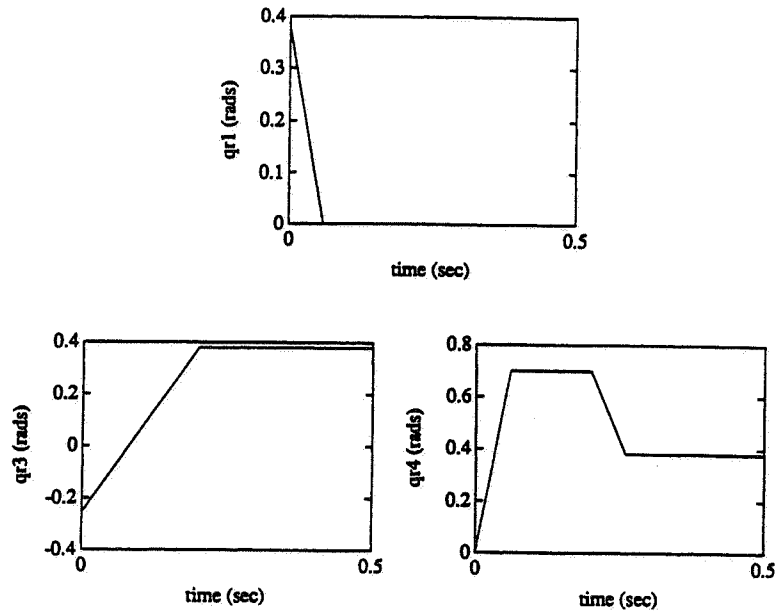

Fig. 6. Reference signals for steady walking on an horizontal plane surface.

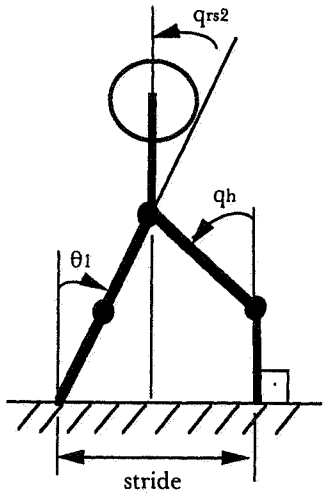

Fig. 7. Biped configuration at the moment where the free end touches the ground.

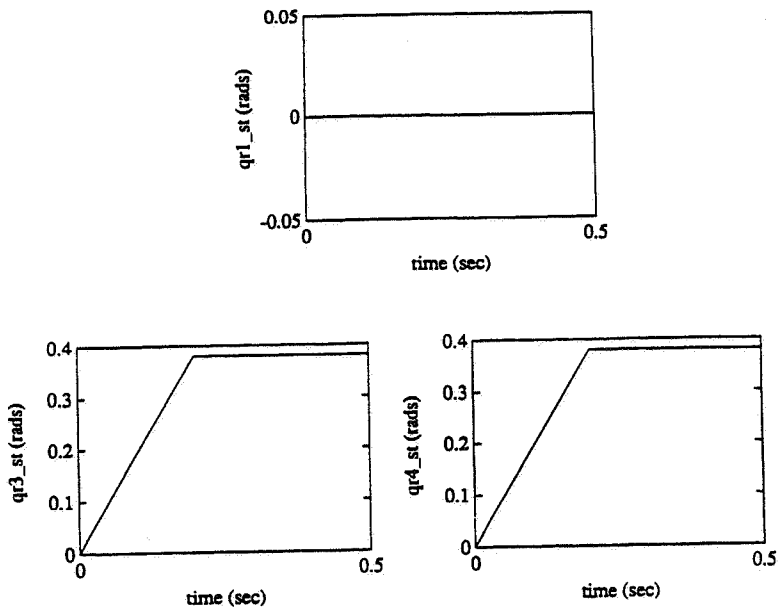

Fig. 8. Reference signals for the starting step (from the vertical position).

Thus, the only parameter that remains for selection is the parameter λ. Here we assume the following:

(i) Maximum control bandwidth 300 rad/sec ($\lambda \leqslant 300$ rad/sec).

(ii) Sampling period $T_s = 2$ msec (i.e. sampling frequency $f_s = 500$ Hz) which is realistic if the algorithm is programmed in ASSEMBLY and all trigonometric functions are stored in the memory.

The results obtained with $\lambda = 100$ are shown in Figures 9a and 9b. Figure 9a shows the tracking error for $0 \leqslant t \leqslant 4$ sec and Figure 9b depicts the error at the collision time ($1 \leqslant t \leqslant 1.5$ sec) of the free end with the ground. Figure 10 shows the torque variations in a small time interval ($1.05 \leqslant t \leqslant 1.2$ sec) around the exchange of the supporting leg. From Figure 9(a, b) one observes that the tracking error is returned to zero after a time period less than or equal to 0.1 sec ($\lambda = 100$ rad/sec implies a time constant $= 1/100$ sec $= 0.01$ sec). The average tracking error for $\lambda = 100$ is 0.0123 rad.

For $\lambda = 150$ the error vanishing period is 0.05 sec and the average tracking error is 0.0070 rad. The corresponding figures for $\lambda = 200$ are 0.04 sec and 0.0014 rad (see Figure 11). The walking mode of the biped on the horizontal surface has the form of Figure 12.

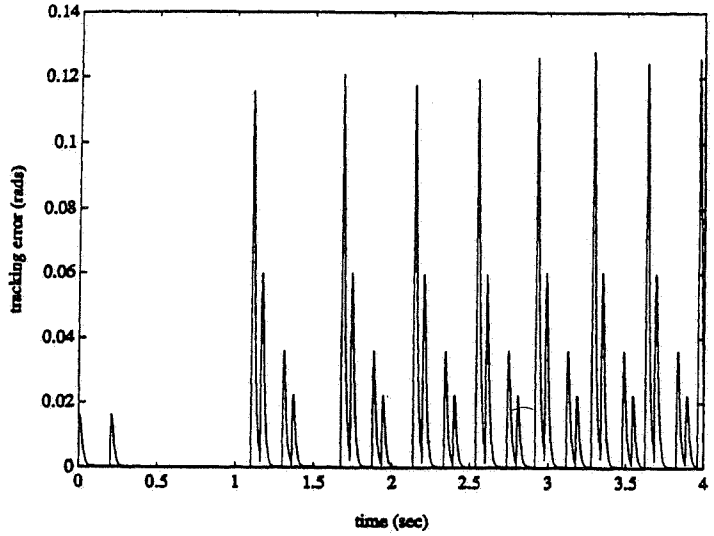

(α)

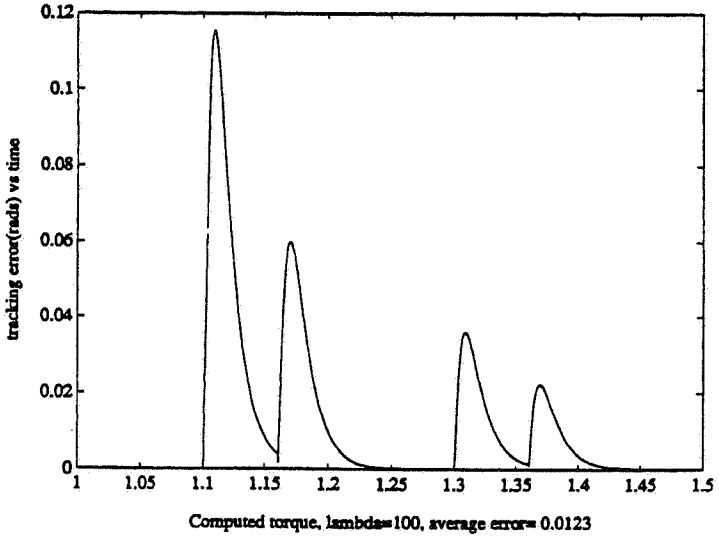

(β)

Fig. 9. Trajectory tracking error obtained with computed torque-control.

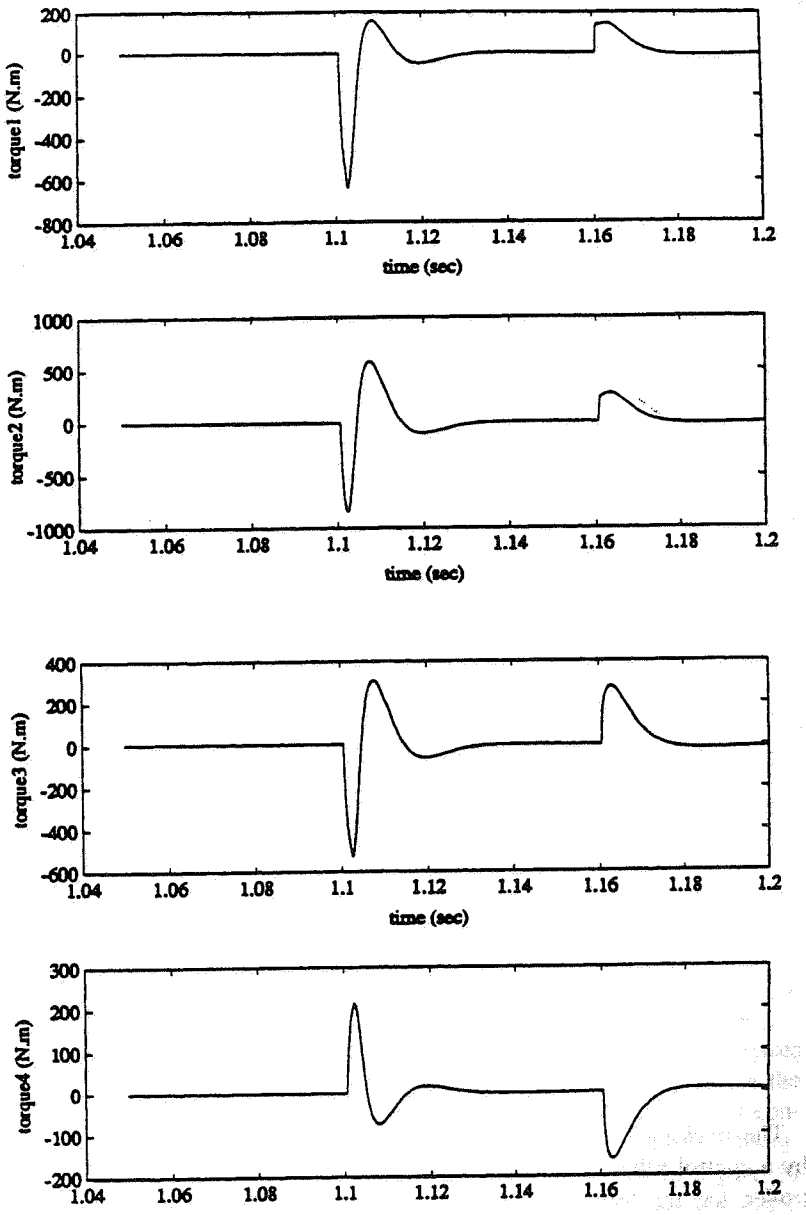

Fig. 10. Driving torques of the four joints corresponding to the computed torque-control ($\lambda = 100$).

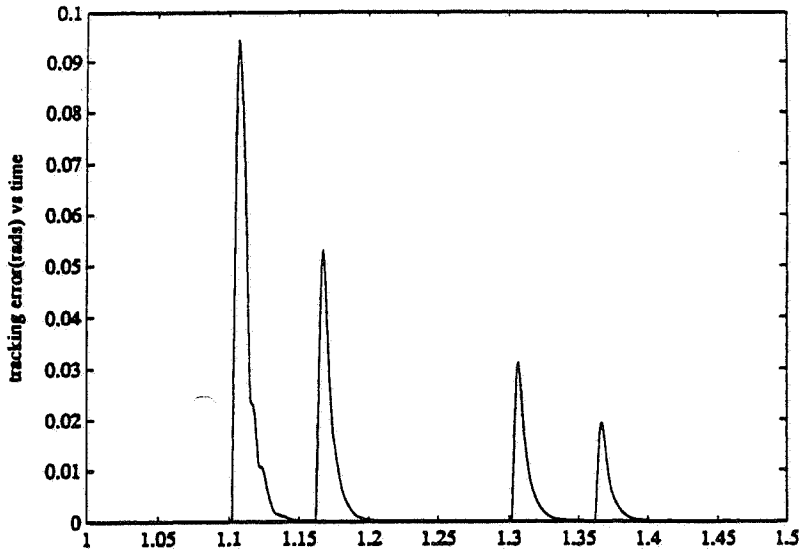

Fig. 11. Tracking error of computed torque-control for $\lambda = 200$.

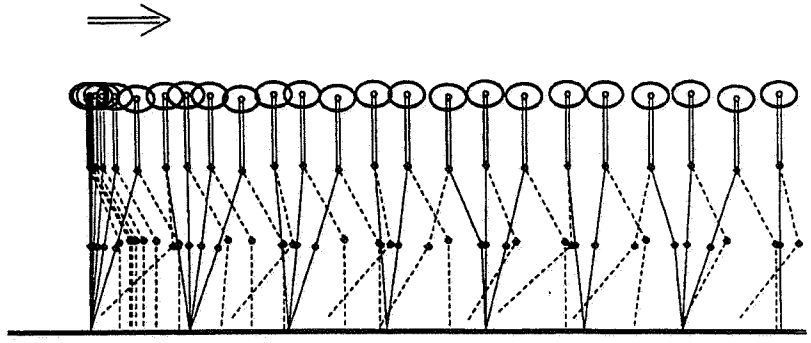

Fig. 12. Locomotion mode of 5-link biped (stick diagram).

The tracking error that was obtained by local (decoupled) PD control, i.e. by a control scheme where each joint is controlled by an independent PD controller, has the form shown in Figure 13. One observes here the existence of a steady-state error (although very small) in contrast with the computed torque-control where the error is always returned to zero in a given finite time. The corresponding average tracking error is now 0.0107 rad. The comparison of Figures 11 and 13 shows the superiority of the computed torque scheme over

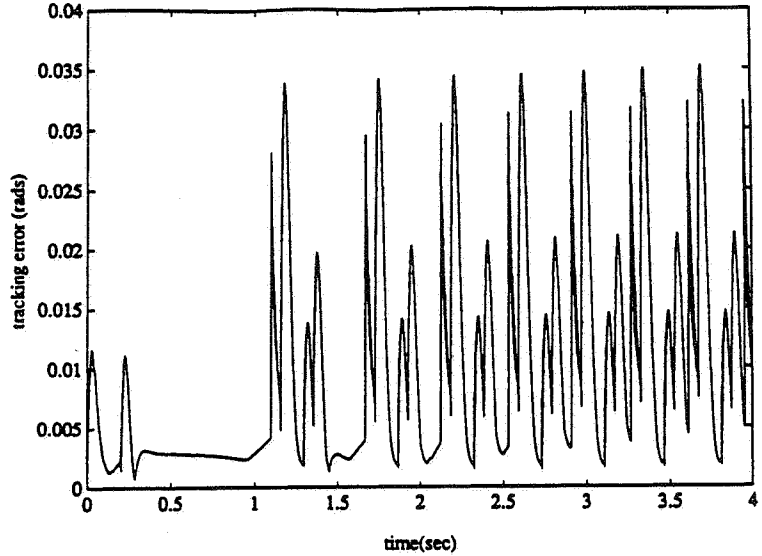

Fig. 13. Tracking error of local PD control for $\lambda = 200$.

Table II. Parameters of a human-sized biped

Link	Mass m_i (kg)	Moment of inertia I_i (kg m)	Length l_i (m)	Location of center of mass d_i (m)
Torso	49.00	2.350	—	0.280
Thigh	7.63	0.089	0.431	0.247
Leg	4.55	0.105	0.502	0.267

the simple local PD scheme. This superiority is strengthened further if we use a biped with the parameters given in Table II which are analogous to those of the human body (masses, moments of inertia and lengths).

The effect of this increase in the model parameters (particularly in the masses and moments of inertia of the biped links) is to obtain a large increase in the tracking errors obtained with local PD control. This is so, since the local control does not take into account the nonlinear structure of the model. The error obtained in this case with the local PD control is depicted in Figure 14 for a time interval 3 sec (average tracking error 0.0359 rad), the angle displacements q_1, q_2, q_3, q_4 in Figure 15, and the driving torques in Figure 16. From Figure 15 one can easily see the difficulty of the system to follow up the desired reference signals. Another undesirable characteristic of the local control is the fact that the biped cannot maintain its body in the vertical po-

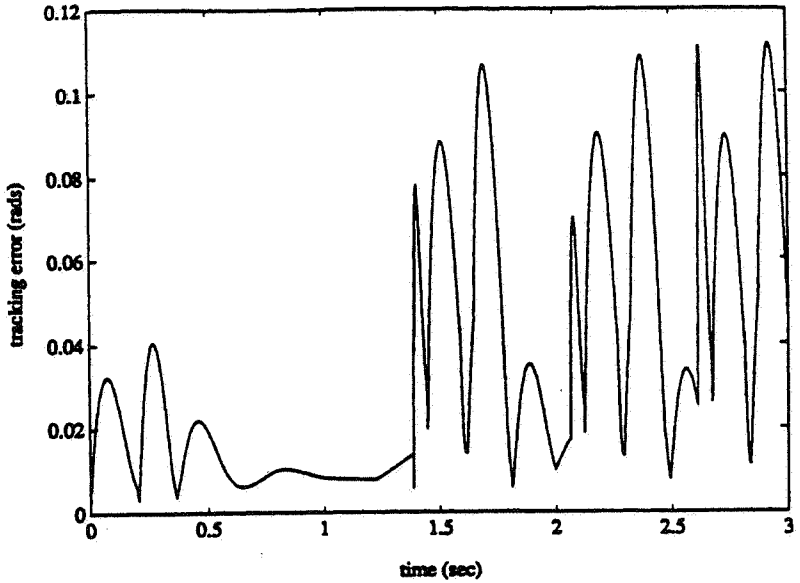

Fig. 14. Tracking error of the human-sized biped for local PD control.

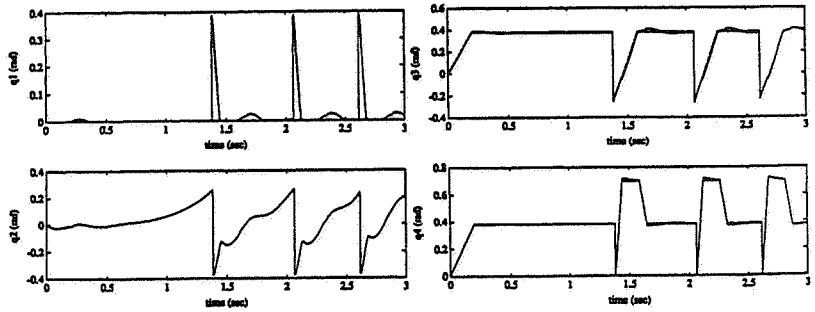

Fig. 15. Angle displacements of the human-sized biped joints with local PD control.

sition (angle θ_3) as it is seen in Figure 17. The results obtained when we apply computed torque control ($\lambda = 150$) to the human-sized biped are shown in Figures 18 and 19. The average tracking error (again over a time period of 3 sec) is 0.0033 rad which is ten time smaller than that obtained with local control. However, this is achieved through driving torques that are about 10 times larger from the ones corresponding to the small-sized biped of Table I.

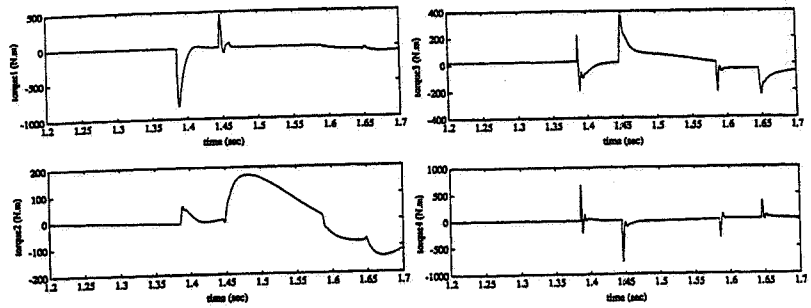

Fig. 16. Driving torques of the human-sized biped with local PD control.

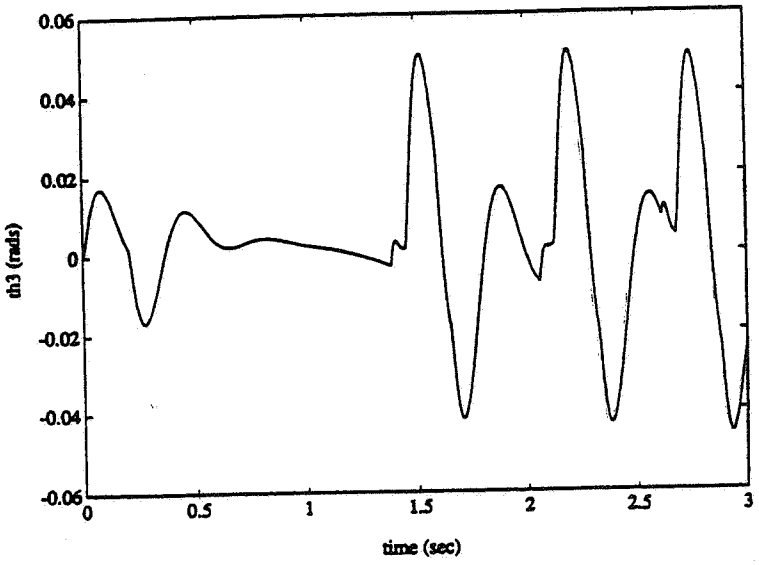

Fig. 17. Variation of the body posture (angle θ_3) with local control.

4.3. STAIR CLIMBING GAIT

Here, the capability of the biped to climb a set of stairs of fixed height h is examined using the computed torque control algorithm. Full knowledge of the biped parameters is assumed and the results presented correspond to $h = 10$ cm. For a gait on a flat horizontal surface the stride is given by (61) where the angle q_{rs2} is given by (60). Thus, the stride on a flat horizontal surface is

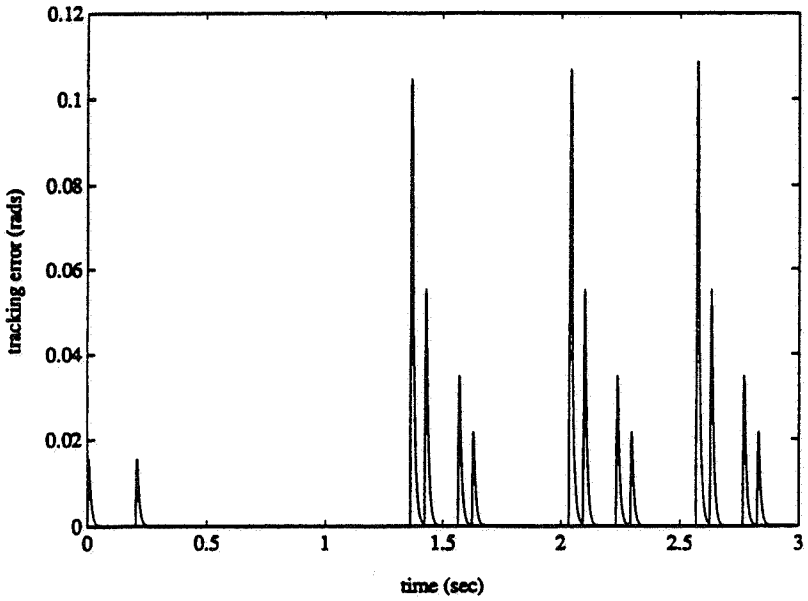

Fig. 18. Tracking error of the human-sized biped with computed torque-control ($\lambda = 150$).

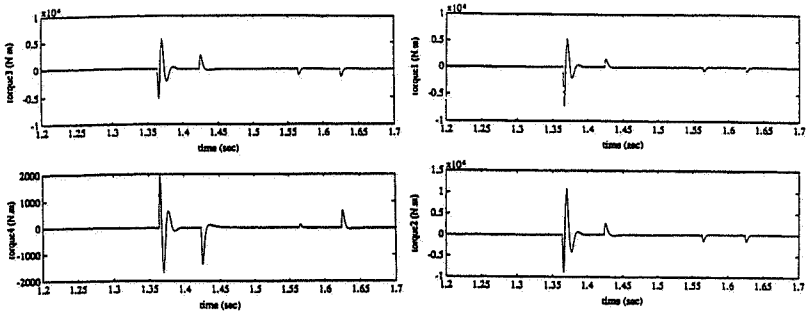

Fig. 19. Driving torques of the human-sized biped with computed torque-control ($\lambda = 150$).

constant and known. To climb a stair in front of it the biped needs to measure (with the aid of suitable sensors) the height difference at the end of the stride, so as to adapt the reference vector signal $q_r(t)$. To enable the biped to climb a stair the reference signals described in Section 4.1 must be modified as follows.

(i) The value $q_{rs3} = q_h$ must be increased sufficiently in order for the free end to overtake the stair obstacle.

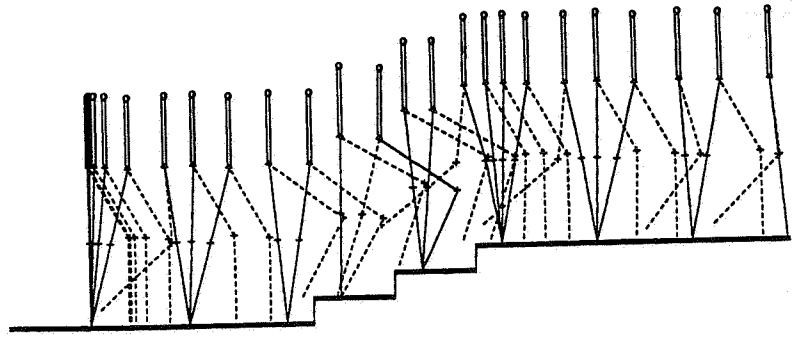

Fig. 20. Biped climbing a sequence of stairs of equal height (10 cm).

(ii) The body is again kept vertical although it could be at a positive angle in order to increase the angular momentum.

(iii) Since in our model there is no ankle joint (which would increase externally the angular momentum in the desired direction) we assume that the angle $q_{r3}(t)$ does not take permanently a constant value during the whole step time, but it starts decreasing, just before the contact of the free leg with the ground, such that at the contact instant to have a velocity towards the ground and the back. In this way the biped achieves the necessary impact for the rise of its center of gravity and the regular gait forward.

With a reference signal that satisfies all the above assumptions, the biped can climb a series of steps as shown pictorially in Figure 20. The path of the center of gravity (coordinates cgx and cgy with respect to the supporting end each time) has the form shown in Figure 21. Finally the trajectories of the joint angles and driving torques have the form of Figures 22 and 23. The above results were achieved with the application of the computed torque-control algorithm with exact knowledge of the biped parameters (i.e. with no uncertainty), and show that our 5-link biped can walk efficiently on a staircase (and consequently on any anomalous surface) provided it has the means to measure the height difference h each time.

4.4. SLIDING MODE CONTROL

Here we shall give the results obtained for the above biped when controlled by a sliding mode controller of the type described in Section 3.3. Thus the controller has the form {see (49)}:

$$u_{i+1} = L_i \cdot [\widehat{u}_i - \overline{k}_i \cdot \text{sat}\,(s_i/\Phi_i)] \qquad (i = 1, \ldots, 4), \tag{61a}$$

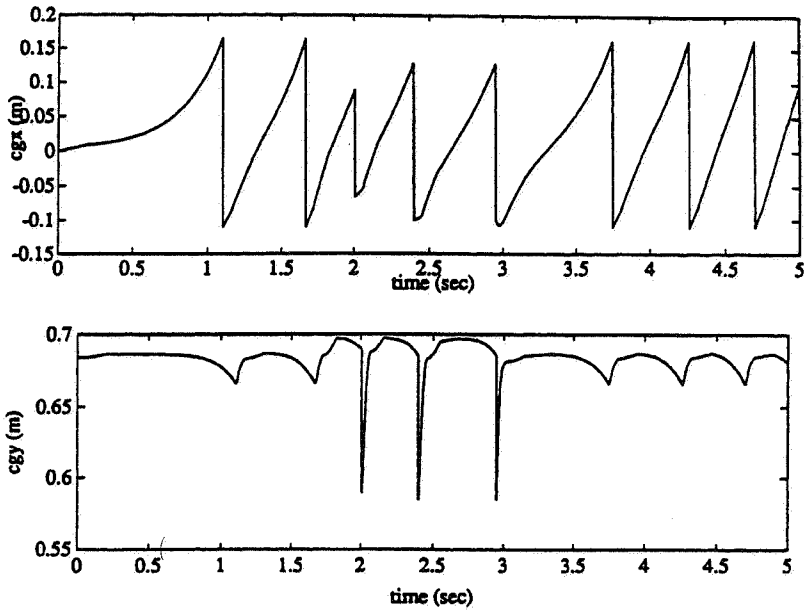

Fig. 21. Variation with time of the position of the center of gravity.

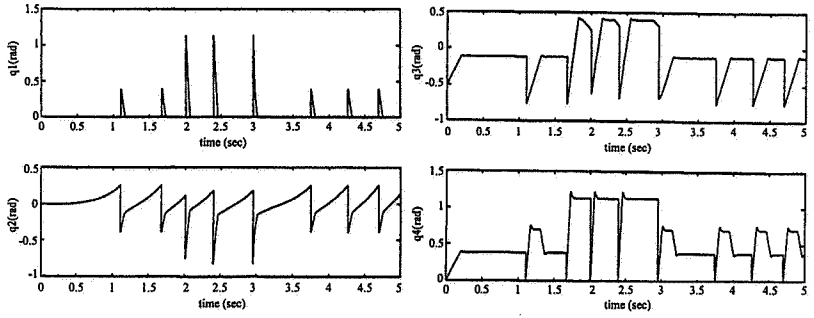

Fig. 22. Trajectories of the joint angles.

where the $\overline{k}_i$'s and $\mathbf{\Phi}_i$'s are defined by the balancing conditions (45) and (46), and the $\widehat{u}_i$'s are given by

$$\widehat{u}_i = \ddot{q}_{ri} - 2\lambda\dot{e}_i - \lambda^2 e_i \qquad (i = 1, 2, 3, 4), \tag{61b}$$

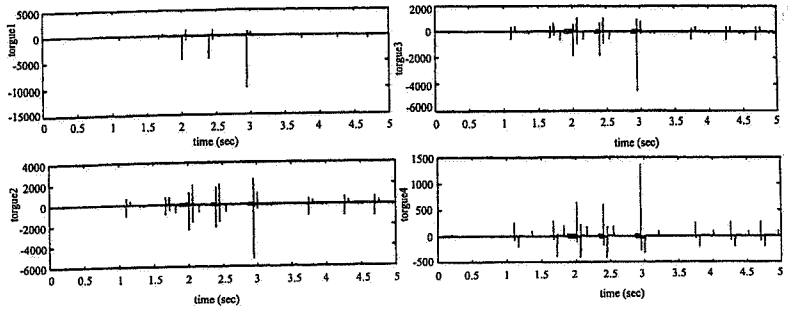

Fig. 23. Variation with time of the corresponding driving torques.

where $e_i = q_i - q_{ri}$. The sliding surfaces in (61a) are selected as

$$s_i = \dot{e}_i + 2\lambda e_i + \lambda^2 \int_t e_i(t')\mathrm{d}t'. \tag{61c}$$

Here, it is assumed that although we do not know the uncertainty in the biped dynamics, we have available some bounds on the uncertainty of the biped parameters (e.g. we know the values of the link masses and moments of inertia with accuracy $\pm e_m \times 100\%$, say 45%). Using these bounds we can compute approximately the scalar quantities $\beta_i^{\min}$ and $\beta_i^{\max}$ with the aid of (55), i.e.

$$0 \leqslant \beta_i^{\min} \leqslant \mathbf{M}_{i+1}^T \widehat{\mathbf{D}}_{q,i+1} \leqslant \beta_i^{\max}, \qquad i = 1, \ldots, 4. \tag{62}$$

For the needs of this relation and for the satisfaction of the condition (54), i.e $\mathbf{M}_i^T \widehat{\mathbf{D}}_{q,i} > 0$, the matrix $\widehat{\mathbf{D}}_q$ is selected to be diagonal and positive definite with elements the diagonal elements of the original matrix $\widehat{\mathbf{D}}_q$. We recall that the vectors $\mathbf{M}_i$ $(i = 1, 2, \ldots, 5)$ are defined by $\mathbf{D}_q^{-1} = [\mathbf{M}_1, \mathbf{M}_2, \ldots, \mathbf{M}_5]$ (see (52a)), the multipliers L_i are given by (56) and the corresponding gain matrix β_i is defined by (57):

$$\beta_i = \left(\beta_i^{\max}/\beta_i^{\min}\right)^{1/2}.$$

The control discontinuity amplitudes $k_i(\mathbf{q}, \dot{\mathbf{q}})$ satisfy the inequalities (58), namely:

$$k_i(\mathbf{q}, \dot{\mathbf{q}}) \geqslant \beta_i \left[\left(1 - \beta_i^{-1}\right) |\widehat{u}_i| + \left(\mathbf{M}_{i+1}^a\right)^T \Delta \mathbf{H}_q^a + \sum_{\substack{j=1 \\ j \neq i}}^{4} L_j |\ddot{q}_{rj}| \left| \mathbf{M}_{i+1}^T \widehat{\mathbf{D}}_{q,j+1} \right| + \eta_i \right], \tag{63}$$

where η_i are positive constants used in the sliding conditions (31), and the elements of $\Delta \mathbf{H}_q^a$, $\mathbf{M}_i^a$ are the absolute values of the elements of $\Delta \mathbf{H}_q$ and $\mathbf{M}_i$, respectively.

Here we use for $\mathbf{M}_i^a$ the estimates $\widehat{\mathbf{M}}_i^a$ that are obtained from the inversion of $\mathbf{D}$. The same is also done to compute $\beta_i^{\min}$ and $\beta_i^{\max}$ in (62), i.e. we set

$$\mathbf{D}_q^{-1} = \mathbf{M} = [\mathbf{M}_1\ \mathbf{M}_2 \cdots \mathbf{M}_5], \qquad \widehat{\mathbf{D}}_q^{-1} = \widehat{\mathbf{M}} = [\widehat{\mathbf{M}}_1\ \widehat{\mathbf{M}}_2 \cdots \widehat{\mathbf{M}}_5]$$

and $\Delta \mathbf{D}_q = \widehat{\mathbf{D}}_q - \mathbf{D}_q$ and obtain

$$\mathbf{M}_i^T \widehat{\mathbf{D}}_{q,i} = \mathbf{M}_i^T \left(\mathbf{D}_{q,i} + \Delta \mathbf{D}_{q,i}\right) = 1 + \mathbf{M}_i^T \Delta \mathbf{D}_{q,i} = 1 + \mathbf{M}_i^T \Delta \widehat{\mathbf{D}}_{q,i}. \tag{64}$$

Now assuming that

$$\widehat{\mathbf{D}}_q = \operatorname{diag}\left[\widehat{D}_{q,ii}\right], \qquad \widehat{\mathbf{M}} = \operatorname{diag}\left[1/\widehat{D}_{q,ii}\right],$$

$$\widehat{\mathbf{M}}_i^T \Delta D_{q,ii} = \frac{\widehat{D}_{q,ii} - D_{q,ii}}{\widehat{D}_{q,ii}} = \frac{\Delta D_q[i,i]}{\widehat{D}_q[i,i]} \tag{65}$$

as explained above, the relations (62), (64) and (65) give

$$\beta_i^{\min} \leqslant 1 + \frac{\Delta D_q[i,i]}{\widehat{D}_q[i,i]} \leqslant \beta_i^{\max}. \tag{66}$$

The quantities $\Delta D_q[i,i]$ can be computed from (12a, c), i.e.

$$\begin{aligned}
\Delta D_q[1,1] &= \Delta A_{11} + \Delta A_{12} + \Delta A_{13} - \Delta A_{14} - \Delta A_{15},\\
\Delta D_q[2,2] &= -\Delta A_{22} - \Delta A_{23} + \Delta A_{24} + \Delta A_{25},\\
\Delta D_q[3,3] &= -\Delta A_{33} + \Delta A_{34} + \Delta A_{35},\\
\Delta D_q[4,4] &= \Delta A_{44} + \Delta A_{45},\\
\Delta D_q[5,5] &= -\Delta A_{55}.
\end{aligned}$$

Also

$$\begin{aligned}
\Delta A_{1j} &= \delta D[1,j] + \delta D[2,j] + \delta D[3,j] - \delta D[4,j] - \delta D[5,j] \qquad (j = 1, \ldots, 5),\\
\Delta A_{2j} &= -\delta D[2,j] - \delta D[3,j] + \delta D[4,j] + \delta D[5,j] \qquad (j = 2, \ldots, 5),\\
\Delta A_{3j} &= -\delta D[3,j] + \delta D[4,j] + \delta D[5,j] \qquad (j = 3, \ldots, 5),\\
\Delta A_{4j} &= \delta D[4,j] + \delta D[5,j] \qquad (j = 4, 5),\\
\Delta A_{5j} &= -\delta D[5,j] \qquad (j = 5).
\end{aligned}$$

The bounds $\delta D[i,j]$ that appear in the above relations can be easily computed using (7) as follows. It is assumed that the link masses of the biped are known with uncertainty $e_m \times 100\%$ $(0 \leqslant e_m < 1)$. Similarly, let e_I, e_l and e_d be the known uncertainties in the moment of inertial I and the parameters l (link length) and d (position of center of mass with respect to the end of the link). Then

$$\begin{aligned}
\Delta D[1,1] &= e_I \cdot \hat{I}_1 + \hat{m}_1 \hat{d}_1^2 \left[\left(1 + e_m\right)\left(1 + e_d\right)^2 - 1\right]\\
&\quad + \left(\hat{m}_2 + \hat{m}_3 + \hat{m}_4 + \hat{m}_5\right) \hat{l}_1^2 \left[\left(1 + e_m\right)\left(1 + e_l\right)^2 - 1\right],\\
\Delta D[2,2] &= e_I \cdot \hat{I}_2 + \hat{m}_2 \hat{d}_2^2 \left[\left(1 + e_m\right)\left(1 + e_d\right)^2 - 1\right]\\
&\quad + \left(\hat{m}_3 + \hat{m}_4 + \hat{m}_5\right) \hat{l}_2^2 \left[\left(1 + e_m\right)\left(1 + e_l\right)^2 - 1\right],\\
\Delta D[3,3] &= e_I \cdot \hat{I}_3 + \hat{m}_3 \hat{d}_3^2 \left[\left(1 + e_m\right)\left(1 + e_d\right)^2 - 1\right],\\
\Delta D[4,4] &= e_I \cdot \hat{I}_4 + \hat{m}_4 \left(\hat{l}_4 - \hat{d}_4\right)^2 \left[\left(1 + e_m\right)\left(1 + e_{ld4}\right)^2 - 1\right]\\
&\quad + \hat{m}_5 \hat{l}_4^2 \left[\left(1 + e_m\right)\left(1 + e_l\right)^2 - 1\right],
\end{aligned}$$

where e_{ld4} is computed as follows

$$\begin{aligned}
&\left(l_4 - d_4\right)^2 - \left(\hat{l}_4 - \hat{d}_4\right)^2\\
&\quad \leqslant \left[\hat{l}_4\left(1 + e_l\right) - \hat{d}_4\left(1 - e_d\right)\right]^2 - \left(\hat{l}_4 - \hat{d}_4\right)^2\\
&\quad = \left[\left(\hat{l}_4 - \hat{d}_4\right) + \left(\hat{l}_4 e_l + \hat{d}_4 e_d\right)\right]^2 - \left(\hat{l}_4 - \hat{d}_4\right)^2\\
&\quad = \left(\hat{l}_4 - \hat{d}_4\right)^2 \left[\left(1 + \frac{\hat{l}_4 e_l + \hat{d}_4 e_d}{\hat{l}_4 - \hat{d}_4}\right)^2 - 1\right].
\end{aligned}$$

Therefore:

$$e_{ld4} = \frac{\hat{l}_4 e_l + \hat{d}_4 e_d}{\hat{l}_4 - \hat{d}_4}.$$

In general e_{ldi} denotes the uncertainty bound for $(l_i - d_i)$ and the following relation holds

$$e_{ldi} = \frac{\hat{l}_i e_l + \hat{d}_i e_d}{\hat{l}_i - \hat{d}_i}.$$

Thus:

$$\Delta D[5,5] = e_I \cdot \hat{I}_5 + \hat{m}_5 (\hat{l}_5 - \hat{d}_5)^2 \left[(1+e_m)(1+e_{ld5})^2 - 1 \right].$$

Also

$$\delta D[i,j] = \delta p_{ij} \qquad (i = 1, \ldots, 4 \quad \text{and} \quad j = i+1, \ldots, 5)$$

and

$$\begin{aligned}
\delta p_{12} &= \hat{m}_2 \hat{l}_1 \hat{d}_2 \left[(1+e_m)(1+e_l)(1+e_d) - 1 \right] \\
&\quad + (\hat{m}_3 + \hat{m}_4 + \hat{m}_5) \hat{l}_1 \hat{l}_2 \left[(1+e_m)(1+e_l)^2 - 1 \right], \\
\delta p_{13} &= \hat{m}_3 \hat{l}_1 \hat{d}_3 \left[(1+e_m)(1+e_l)(1+e_d) - 1 \right], \\
\delta p_{14} &= \hat{m}_4 \hat{l}_1 (\hat{l}_4 - \hat{d}_4) \left[(1+e_m)(1+e_l)(1+e_{ld4}) - 1 \right] \\
&\quad + \hat{m}_5 \hat{l}_1 \hat{l}_4 \left[(1+e_m)(1+e_l)^2 - 1 \right], \\
\delta p_{15} &= \hat{m}_5 \hat{l}_1 (\hat{l}_5 - \hat{d}_5) \left[(1+e_m)(1+e_l)(1+e_{ld5}) - 1 \right].
\end{aligned}$$

In the same way one can compute the bounds δp_{23}, δp_{24}, δp_{25}, δp_{34}, δp_{35} and δp_{45}. We see therefore that the quantities $\Delta D_q[i,i]$ $(i = 1, 2, \ldots, 5)$ can be computed using the above relations. Thus using (66), the bounds $\beta_i^{\min}$ and $\beta_i^{\max}$ that provide suitable measures for the intervals of parametric uncertainty in the biped inertia matrix $\mathbf{D}_q$, can be computed.

The quantities $\beta_i^{\min}$ and $\beta_i^{\max}$ can also be computed using *a priori* values for e_m, e_I, e_l, and e_d according to the existing uncertainty in the values of m_i, I_i, l_i and d_i. The results that are given in the sequel have been obtained by using the following *a priori* values: $e_m = e_I = 0.45$, $e_l = 0.10$ and $e_d = 0.20$ i.e. a dominating uncertainty in the mass and moment of inertia parameters and a smaller uncertainty in the distance parameters. We first compute $\beta_i^{\min}$ and $\beta_i^{\max}$ and then the quantities $L_i = (\beta_i^{\min} \beta_i^{\max})^{-1/2}$ and $\beta_i = (\beta_i^{\min} / \beta_i^{\max})^{1/2}$. Then using L_i and β_i we compute the amplitudes k_i of the control discontinuity using (63). It only remains to compute the bounds $\Delta \mathbf{H}_q^a$ which are required

in (63). To this end, the following relations are used:

$$\begin{aligned}
\Delta \mathbf{H}_q^a &= \Delta \mathbf{h}_q^a + \Delta \mathbf{G}_q^a, \\
|\Delta h_{q0}| &= |\Delta h_1| + |\Delta h_2| + |\Delta h_3| + |\Delta h_4| + |\Delta h_5|, \\
|\Delta G_{q0}| &= |\Delta G_1| + |\Delta G_2| + |\Delta G_3| + |\Delta G_4| + |\Delta G_5|, \\
|\Delta h_{q1}| &= |\Delta h_2| + |\Delta h_3| + |\Delta h_4| + |\Delta h_5|, \\
|\Delta G_{q1}| &= |\Delta G_2| + |\Delta G_3| + |\Delta G_4| + |\Delta G_5|, \\
|\Delta h_{q2}| &= |\Delta h_3| + |\Delta h_4| + |\Delta h_5|, \\
|\Delta G_{q2}| &= |\Delta G_3| + |\Delta G_4| + |\Delta G_5|, \\
|\Delta h_{q3}| &= |\Delta h_4| + |\Delta h_5|, \\
|\Delta G_{q3}| &= |\Delta G_4| + |\Delta G_5|,
\end{aligned}$$

and

$$\begin{aligned}
|\Delta h_{q4}| &= |\Delta h_5|, \\
|\Delta G_{q4}| &= |\Delta G_5|.
\end{aligned}$$

The quantities Δh_i and ΔG_i $(i = 1, 2, \ldots, 5)$ are computed using (12a) and the quantities δp_{ij} computed above. For example

$$\begin{aligned}
|\Delta h_1| &= |\Delta h_{122}| \dot{\theta}_{2,\max}^2 + |\Delta h_{133}| \dot{\theta}_{3,\max}^2 + |\Delta h_{144}| \dot{\theta}_{4,\max}^2 + |\Delta h_{155}| \dot{\theta}_{5,\max}^2 \\
&\leqslant (\delta p_{12} + \delta p_{13} + \delta p_{14} + \delta p_{15}) (\dot{\theta}_{\max})^2.
\end{aligned}$$

Finally, we have to set a value for η_i which determines the convergence rate to the boundary layer. Here the value $\eta_i = \eta = 30$ is selected which ensures a sufficiently high convergence rate. Also, since the number of calculations in the present case does not differ very much from the one of the computed torque it is sufficient to use again the sampling time $T_s = 2$ msec. The quantities $\overline{k}_i$ and $\mathbf{\Phi}_i$ required in (61a) are computed using the balancing conditions. To summarize the values of the parameters used for the results shown in Figures 24 through 28 are given in Table III.

Figures 24a and 24b show the variation of the tracking error $|e_1(t)| + |e_2(t)| + |e_3(t)| + |e_4(t)|$ in an interval of 3 sec and around the time of completion of the first step, respectively. The average tracking error for the first two steps is equal to 0.0025 rad. One can observe that the error returns to zero despite the existence of parametric uncertainty. Figure 25 shows the variation of s_i $(i = 1, 2, 3, 4)$

Table III. Parameter values for the sliding mode control

e_m	e_I	e_l	e_d	η	T_s	λ
0.45	0.45	0.10	0.20	0.30	2 msec	150

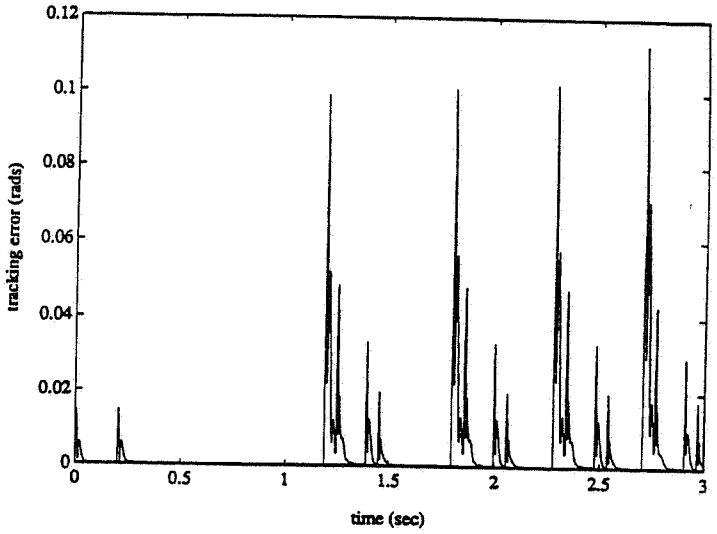

(α)

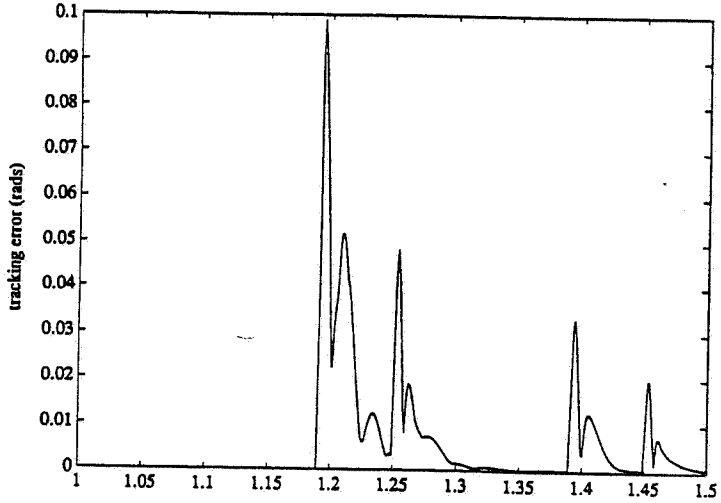

(β)

Fig. 24. Tracking error of the sliding mode control with 45% parametric uncertainty and $\lambda = 150$.

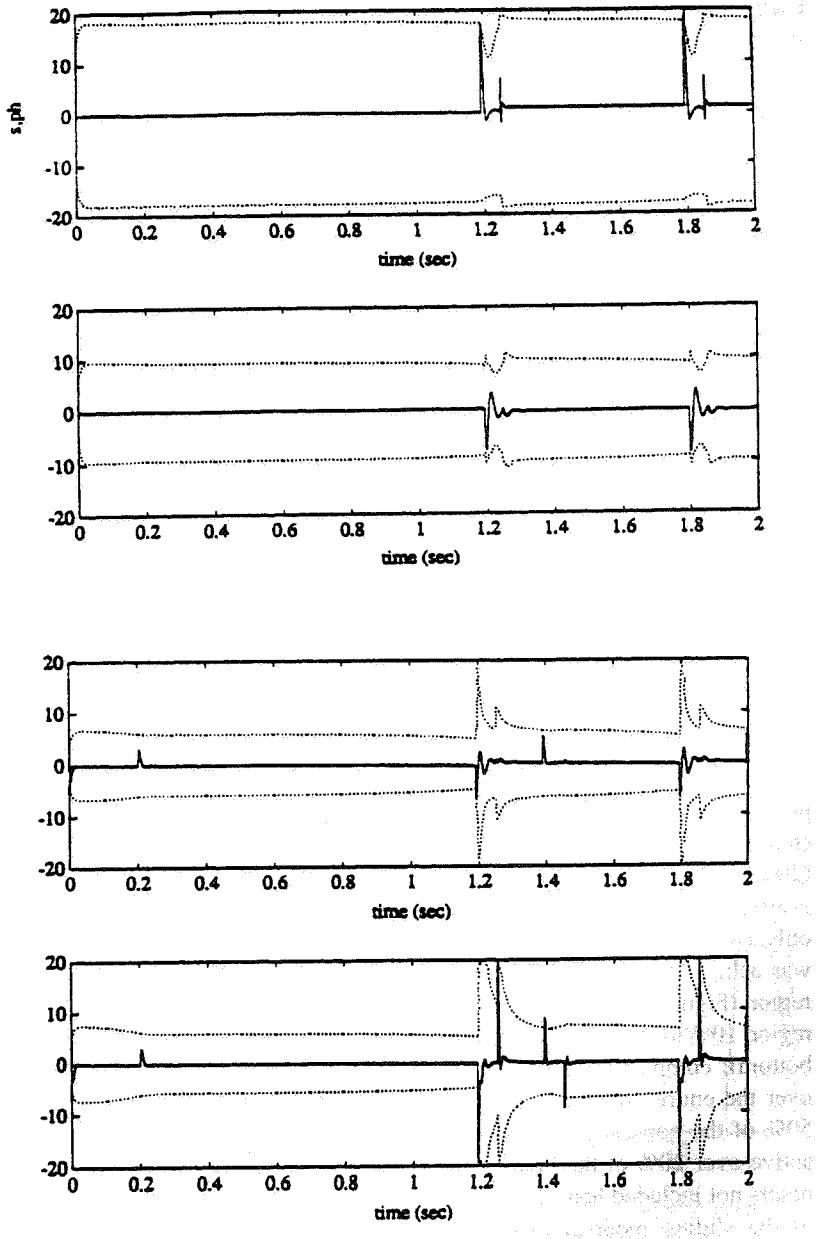

Fig. 25. Trajectory of the error sliding function $s(t)$.

within the boundary layer $[-\Phi_i(t),\ +\Phi_i(t)]$. These diagrams contain useful information since the Φ_i's provide an estimate of the parametric uncertainty at each time, and the s_i's give a measure of the trajectory tracking error. Figure 26 depicts the variation of the angular displacements of the four joints in a time interval of 3 sec, from which one can see the very good tracking of the desired reference signals despite the presence of the uncertainty. Finally, Figures 27 and 28 show the driving torques of the biped in a 3-sec interval and at the completion time of the first step, respectively. One can observe the increased values of these torques in order to be able to face the existing parametric uncertainty.

4.5. COMPARISON OF SLIDING MODE WITH COMPUTED TORQUE-CONTROL

Here, the results of the sliding mode control presented in Section 4.4 will be compared with those obtained for the same parameter set (Table III) via computed torque control. The results obtained using the computed torque control are depicted in Figures 29, 30 and 31. Comparing Figures 24 and 29 one observes the considerably increased overshoot and the existence of nonzero steady-state error in the computed torque case. The average tracking error (0.0048 rad) of the computed torque for the first two steps is twice the corresponding error (0.0025 rad) of the sliding mode control. Thus in overall for the same control bandwidth $\lambda = 150$ (a fact that is also seen in Figures 28 and 31 where the rate of change of the driving torques is comparable) the results obtained through sliding mode control are much better than those obtained via computed torque (smaller overshoot, zero final value of error, much smaller average tracking error).

The above comparison was made for the parameter uncertainty values $e_m = e_I = 0.45$, $e_l = 0.10$ and $e_d = 0.20$. However, for a full study, this comparison must be made for a sequence of increasing parametric uncertainty. Since the primary source of uncertainty is in the masses and moments of inertia, this study was made by increasing the values of e_m and e_I from 0.10 (10%) to 2.0 (200%) monitoring in each case the average tracking error. To avoid excessive oscillations of the biped motion, the integration of tracking error is carried out only over a region around the sliding surface $s = 0$. The best performance was achieved when the integration was restricted to 20% of the boundary layer region (Figures 32, 33). The average tracking error obtained over the uncertainty region 10% to 200% is depicted in Figure 34 for the following cases (from top to bottom): computed torque-control, sliding mode-control with integral term active over the entire region of s, sliding mode-control with integral term active over 50% of the boundary layer region, and sliding mode-control with integral term active over 20% of the boundary layer. The results presented above (as well as others not included here) have fully verified the theoretically expected superiority of the sliding mode-control over the computed torque-control, especially for situations where there exist large parametric uncertainty.

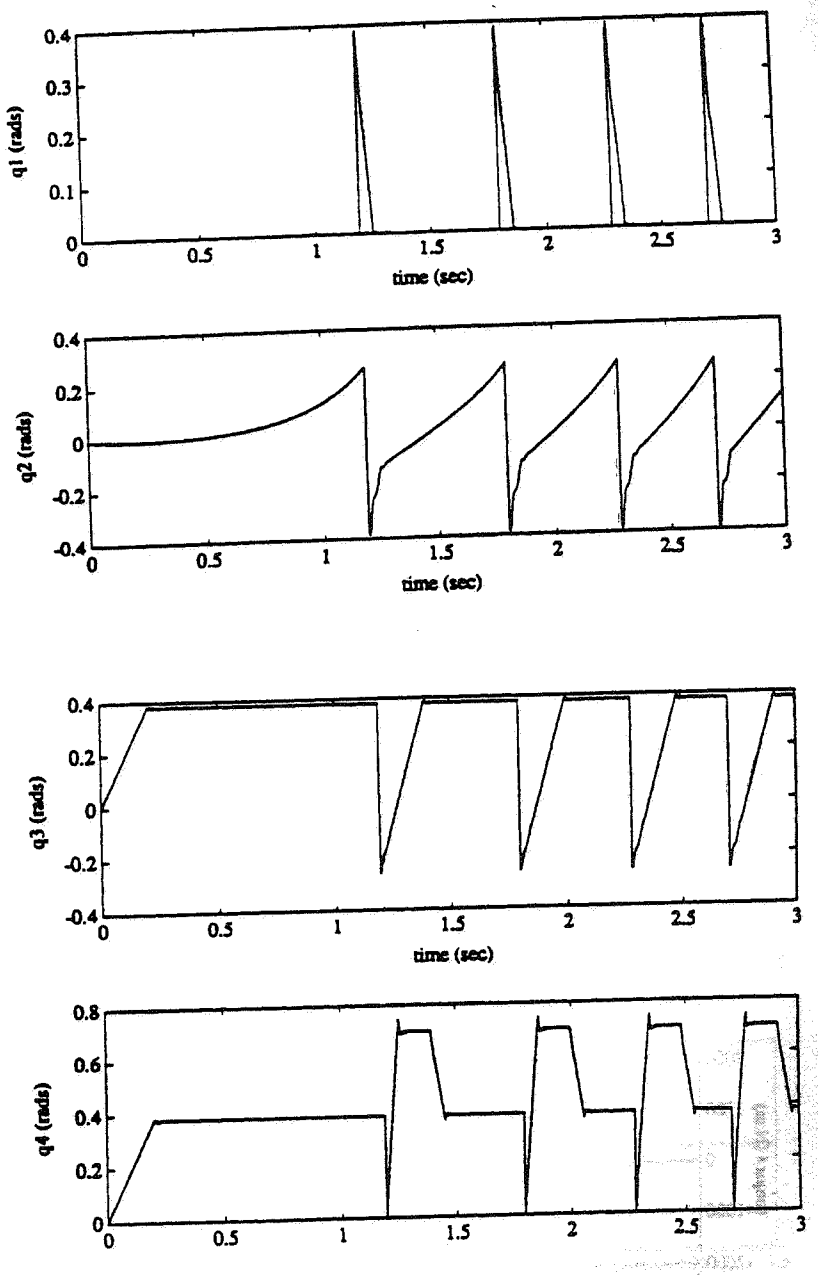

Fig. 26. Joint angle trajectories of sliding mode control with $\lambda = 150$ and 45% uncertainty.

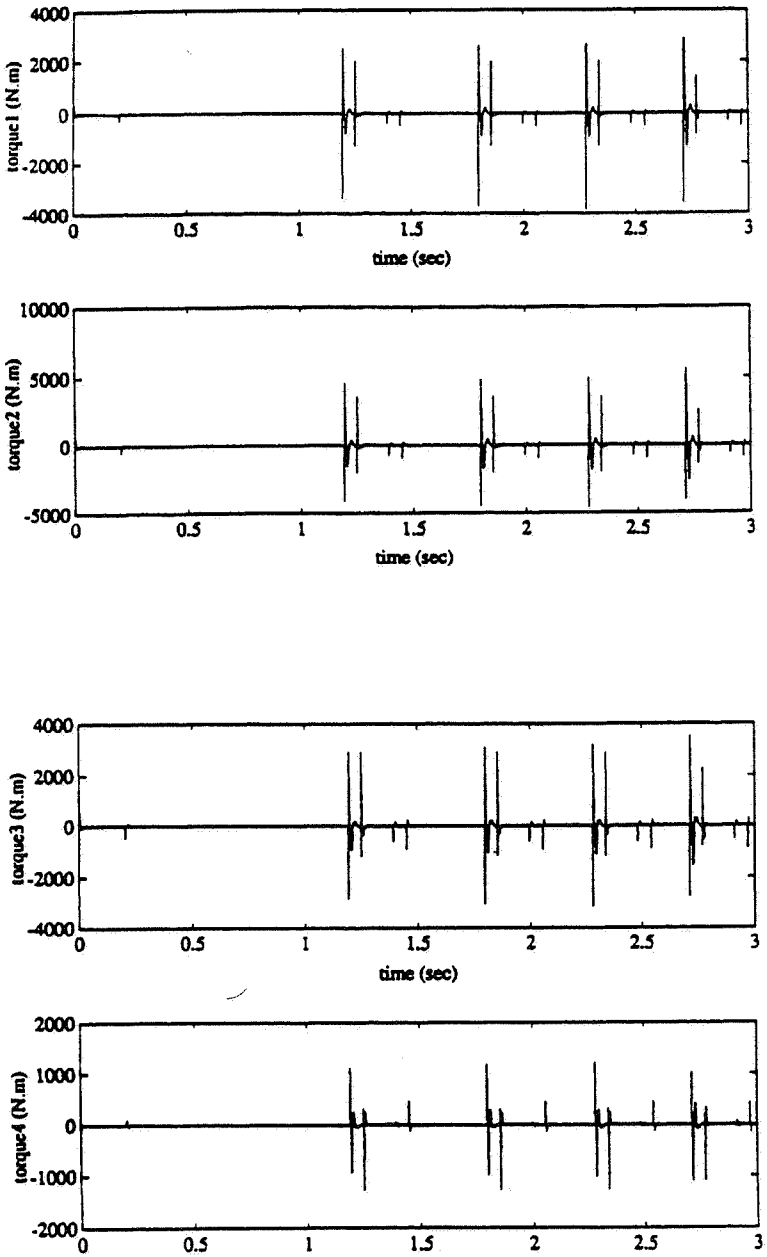

Fig. 27. Driving torques of the biped under sliding mode control ($\lambda = 150$) for 45% uncertainty.

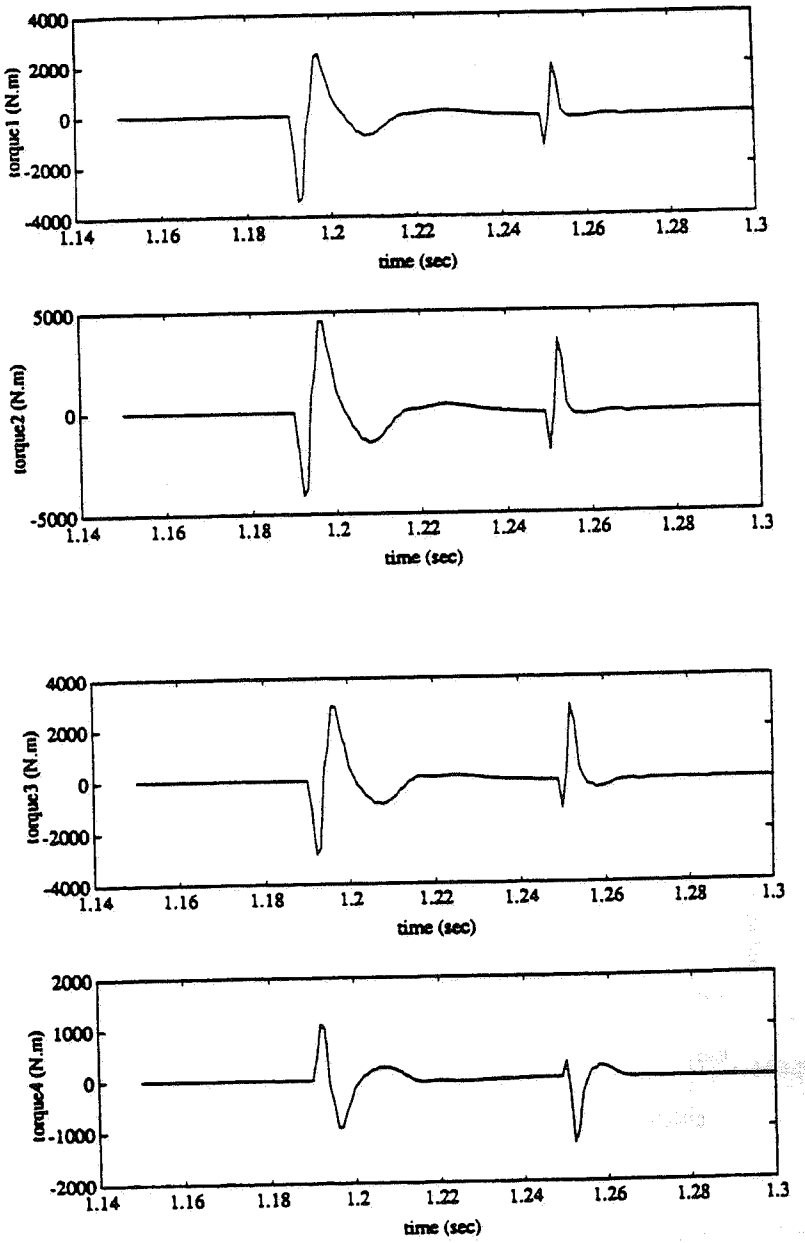

Fig. 28. Driving torques of sliding mode control at the changeover of the supporting leg.

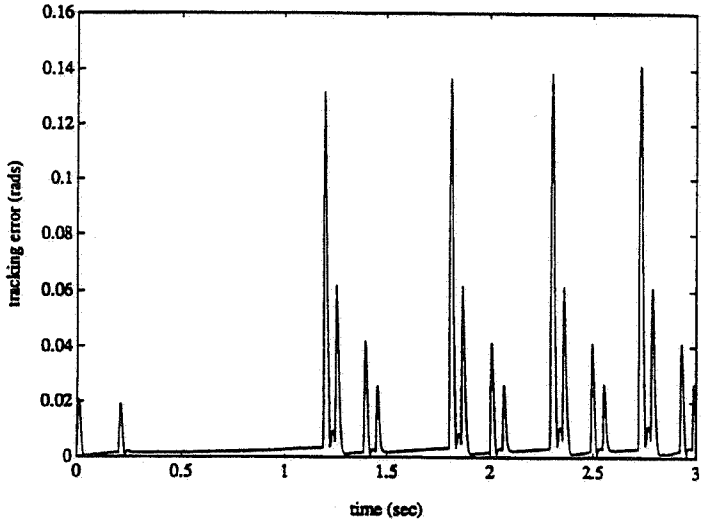

(α)

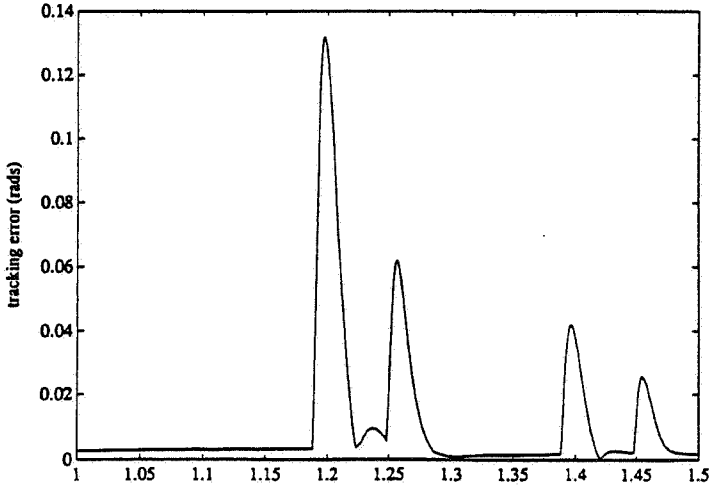

(β)

Fig. 29. Computed torque with $\lambda = 150$ under 45% uncertainty.

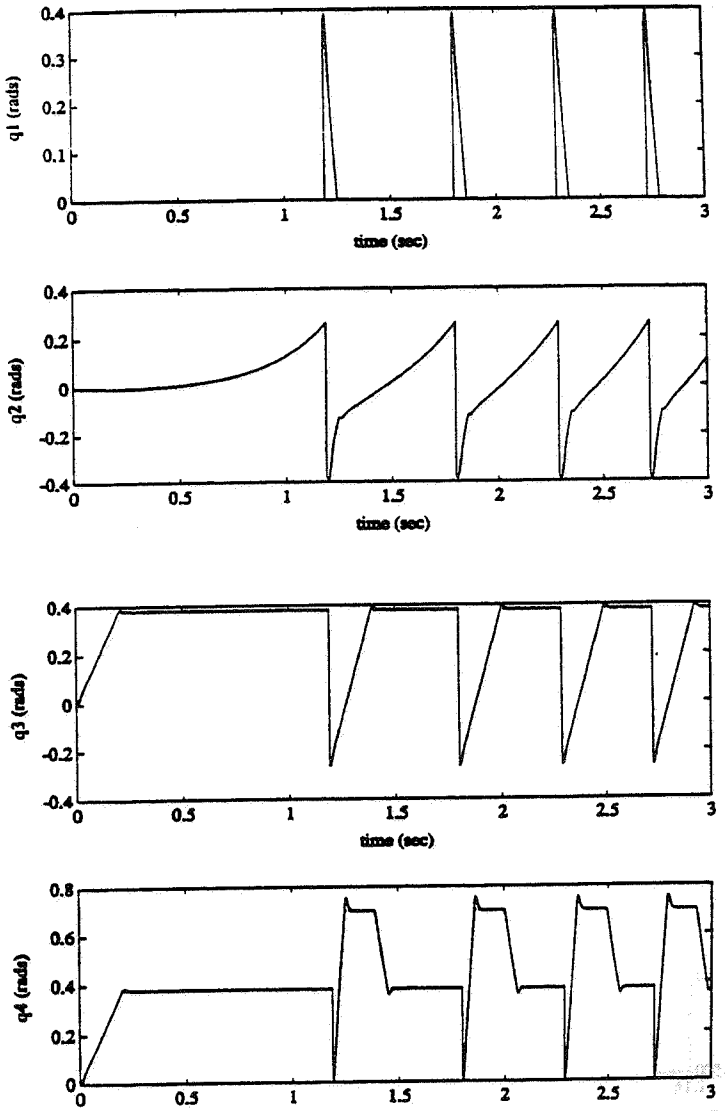

Fig. 30. Joint angles during the steady walk on an horizontal plane under computed torque-control with $\lambda = 150$ and 45% uncertainty.

5. Conclusions

In this paper the effectiveness of robust sliding-mode control applied to a 5-link biped robot was studied and compared to that of the usual computed torque-

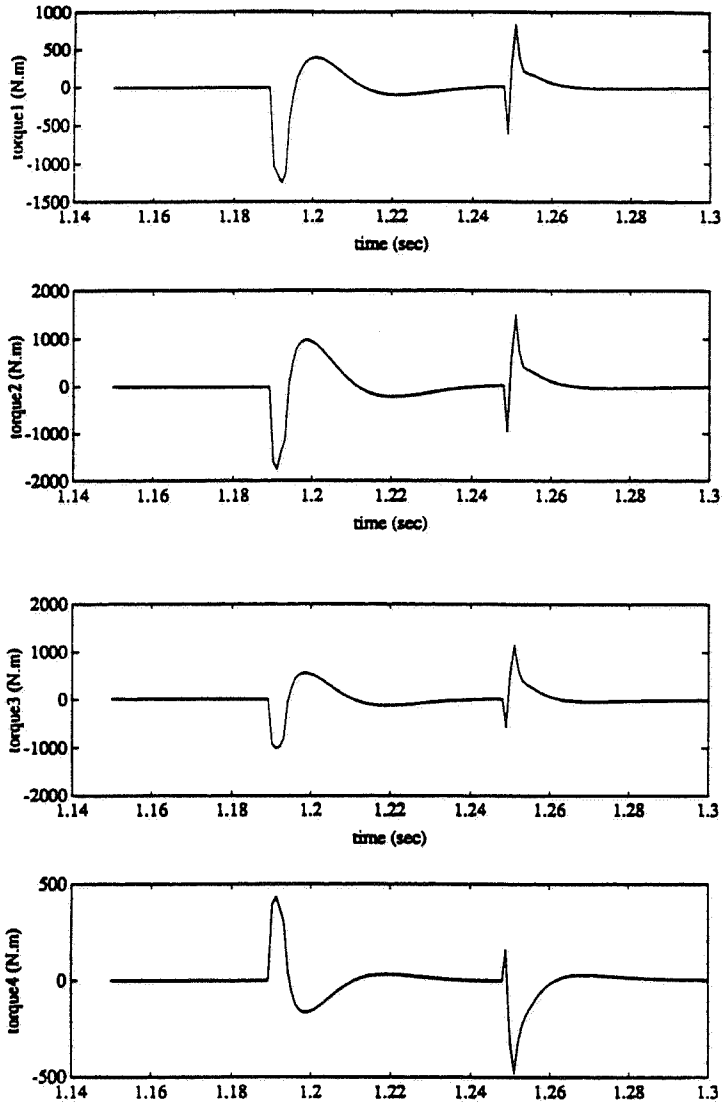

Fig. 31. Driving torques during steady walk on an horizontal plane under computed torque-control with $\lambda = 150$ and 45% uncertainty.

control. The theoretical expectation that sliding mode-control is much superior than computed torque-control in the presence of strong parametric uncertainty was fully verified. The fact that this superiority is strengthened as the uncertainty level of the biped model increases was also established. Through the selection

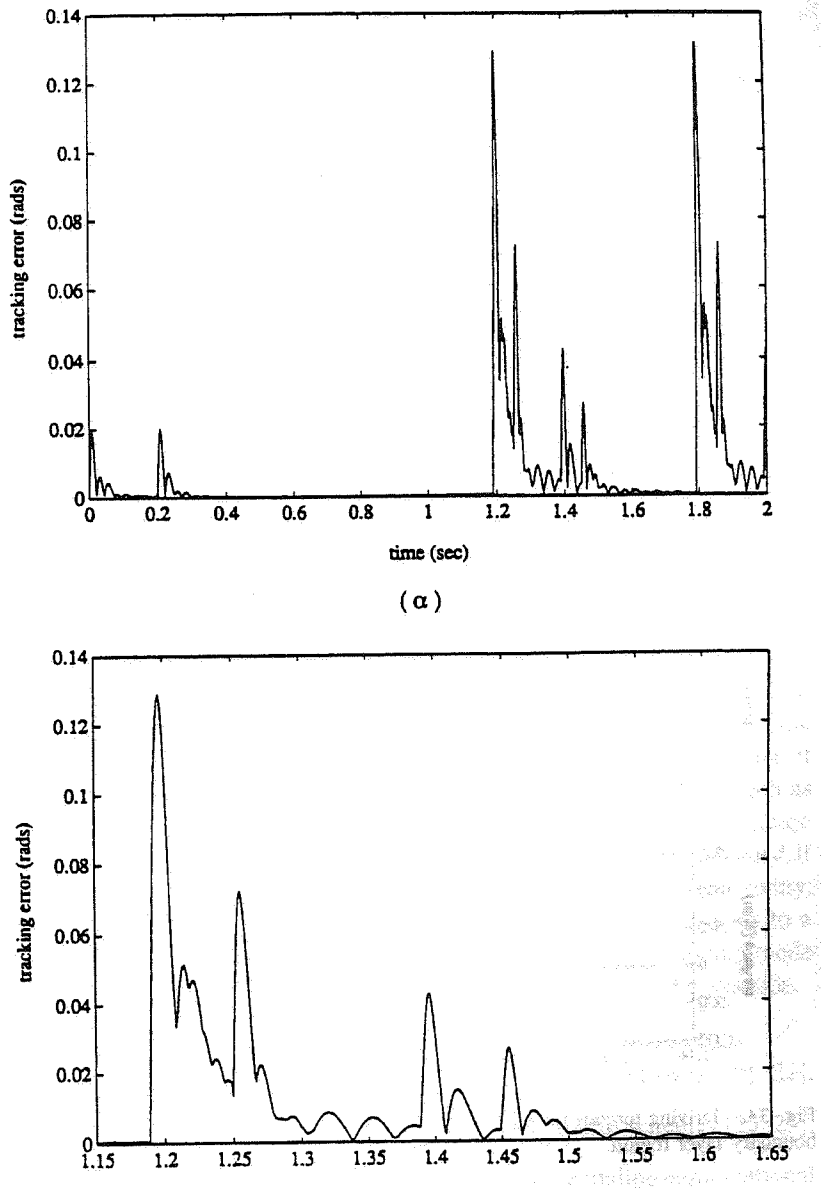

Fig. 32. Tracking error for uncertainty about 200% and integration active over 20% of the boundary layer region.

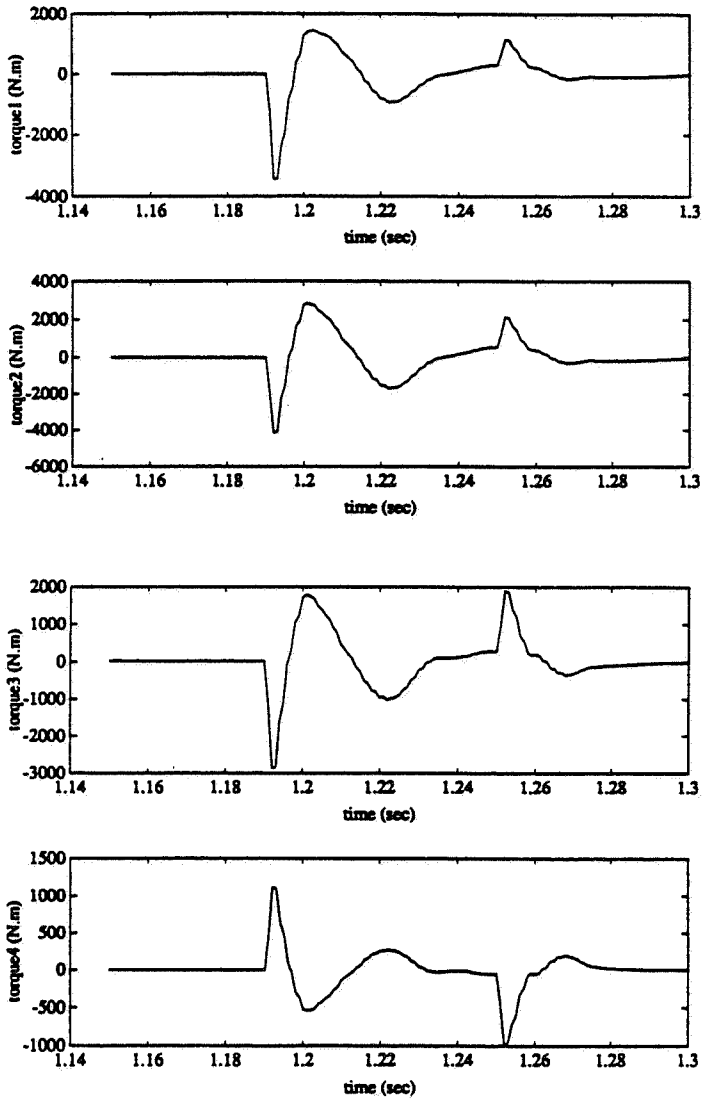

Fig. 33. Driving torques for uncertainty about 200% and integration active over 20% of the boundary layer region.

of appropriate reference signals a stable walk of the biped, both on an horizontal plane surface and on a staircase, has been achieved. It has been observed that if the uncertainty level is very high (higher than 80%) it may not be possible to maintain a stable gait with usual PID control. The computational complexity

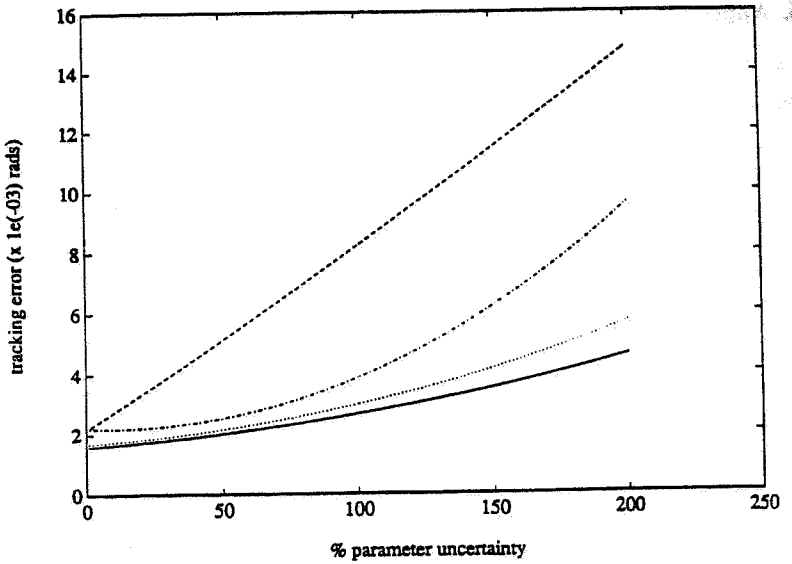

Fig. 34. Comparison of the robustness (represented by the average tracking error) of the various control techniques.

of both the computed torque and the sliding mode-control allow their realization with standard microprocessor hardware and software. In particular, if the algorithms are programmed in *assembly*, the computation time is of the order of 3–4 msec. Further, by using suitable fast inverse dynamics algorithms (such as the Luh–Walker–Paul algorithm) or by parallelizing the computations, this figure can go down to less than 1–2 msec. Another improvement can be obtained if all the trigonometric functions are prestored and called from a ROM memory. Thus, since a sampling frequency of at least 60 Hz ($T_s \leqslant 16$ msec) leads to a very good trajectory tracking performance, it can be argued that the sliding mode control is suitable for use in experimental and practical biped robotic systems.

Work is in progress in the following directions:

- to explore biped models with more links (e.g. 9 links or 11 links) [21–22],
- to explore the performance of alternative robust control schemes [23–25],
- to explore the benefits obtained by using parallel scheduling computational algorithms [26],
- to explore the effectiveness of robust control to handle the situation where one or more robotic arms are attached on the body, considering the effect of their motion as uncertainty to the biped locomotion model.

6. Appendices

6.1. APPENDIX 1. DERIVATION OF THE BIPED DYNAMIC MODEL (5)

The model (5) is derived by applying the Langrange equation of motion

$$\frac{\mathrm{d}}{\mathrm{d}t}\left\{\frac{\partial K}{\partial \dot{q}_i}\right\} - \frac{\partial K}{\partial q_i} + \frac{\partial U}{\partial q_i} = Q_i \qquad (i = 1, 2, \ldots, 5), \tag{A1}$$

where K and U are the total kinetic and total potential energy of the biped, respectively. The potential energy of the biped (Figure 2) is equal to:

$$\begin{aligned} U = {} & m_1 g d_1 \cos\theta_1 \\ & + m_2 g\left(l_1 \cos\theta_1 + d_2 \cos\theta_2\right) \\ & + m_3 g\left(l_1 \cos\theta_1 + l_2 \cos\theta_2 + d_3 \cos\theta_3\right) \\ & + m_4 g\left[l_1 \cos\theta_1 + l_2 \cos\theta_2 - \left(l_4 - d_4\right)\cos\theta_4\right] \\ & + m_5 g\left[l_1 \cos\theta_1 + l_2 \cos\theta_2 - l_4 \cos\theta_4 - \left(l_5 - d_5\right)\cos\theta_5\right] \end{aligned}$$

and so

$$\frac{\partial U}{\partial \theta_1} = -\left[m_1 d_1 + \left(m_2 + m_3 + m_4 + m_5\right) l_1\right] g \sin\theta_1, \tag{A2a}$$

$$\frac{\partial U}{\partial \theta_2} = -\left[m_2 d_2 + \left(m_3 + m_4 + m_5\right) l_2\right] g \sin\theta_2, \tag{A2b}$$

$$\frac{\partial U}{\partial \theta_3} = -\left[m_3 d_3\right] g \sin\theta_3, \tag{A2c}$$

$$\frac{\partial U}{\partial \theta_4} = \left[m_4\left(l_4 - d_4\right) + m_5 l_4\right] g \sin\theta_4, \tag{A2d}$$

$$\frac{\partial U}{\partial \theta_5} = \left[m_5\left(l_5 - d_5\right)\right] g \sin\theta_5. \tag{A2e}$$

The kinetic energy of link i is given by

$$K_i = \frac{1}{2} m_i \mathbf{v}_{ci}^2 + \frac{1}{2} I_i \left(\dot{\theta}_i\right)^2 \qquad (i = 1, \ldots, 5),$$

where $\mathbf{v}_{ci} = [\dot{x}_{ci},\ \dot{y}_{ci}]^T$ is the linear velocity of the center of mass of this link. In the present case one has the following:

$$K_1 = \frac{1}{2}\left(I_1 + m_1 d_1^2\right)\left(\dot{\theta}_1\right)^2, \tag{A3a}$$

$$\mathbf{v}_{c2} = \begin{pmatrix} l_1 \cos\theta_1 \\ -l_1 \sin\theta_1 \end{pmatrix}\dot{\theta}_1 + \begin{pmatrix} d_2 \cos\theta_2 \\ -d_2 \sin\theta_2 \end{pmatrix}\dot{\theta}_2 \Longrightarrow$$

$$\begin{aligned} K_2 = {} & \frac{1}{2}\left(I_2 + m_2 d_2^2\right)\left(\dot{\theta}_2\right)^2 + \frac{1}{2}\left(m_2 l_1^2\right)\left(\dot{\theta}_1\right)^2 \\ & + \left(m_2 d_2 l_1\right)\cos\left(\theta_1 - \theta_2\right)\dot{\theta}_1\dot{\theta}_2, \end{aligned} \tag{A3b}$$

$$\mathbf{v}_{c3} = \begin{pmatrix} l_1 \cos\theta_1 \\ -l_1 \sin\theta_1 \end{pmatrix}\dot{\theta}_1 + \begin{pmatrix} l_2 \cos\theta_2 \\ -l_2 \sin\theta_2 \end{pmatrix}\dot{\theta}_2 + \begin{pmatrix} d_3 \cos\theta_3 \\ -d_3 \sin\theta_3 \end{pmatrix}\dot{\theta}_3 \Longrightarrow$$

$$\begin{aligned} K_3 = {} & \frac{1}{2}\left(I_3 + m_3 d_3^2\right)\left(\dot{\theta}_3\right)^2 \\ & + \frac{1}{2} m_3 \{ l_1^2\left(\dot{\theta}_1\right)^2 + l_2^2\left(\dot{\theta}_2\right)^2 + 2 l_1 l_2 \dot{\theta}_1\dot{\theta}_2 \cos\left(\theta_1 - \theta_2\right) \\ & + 2 l_1 d_3 \dot{\theta}_1\dot{\theta}_3 \cos\left(\theta_1 - \theta_3\right) + 2 l_2 d_3 \dot{\theta}_2\dot{\theta}_3 \cos\left(\theta_2 - \theta_3\right)\}, \end{aligned} \tag{A3c}$$

$$\mathbf{v}_{c4} = \begin{pmatrix} l_1 \cos\theta_1 \\ -l_1 \sin\theta_1 \end{pmatrix}\dot{\theta}_1 + \begin{pmatrix} l_2 \cos\theta_2 \\ -l_2 \sin\theta_2 \end{pmatrix}\dot{\theta}_2 + \begin{pmatrix} \left(l_4 - d_4\right)\cos\theta_4 \\ \left(l_4 - d_4\right)\sin\theta_4 \end{pmatrix}\dot{\theta}_4 \Longrightarrow$$

$$\begin{aligned} K_4 = {} & \frac{1}{2}\left[I_4 + m_4\left(l_4 - d_4\right)^2\right]\left(\dot{\theta}_4\right)^2 \\ & + \frac{1}{2} m_4 \{ l_1^2\left(\dot{\theta}_1\right)^2 + l_2\left(\dot{\theta}_2\right)^2 + 2 l_1 l_2 \dot{\theta}_1\dot{\theta}_2 \cos\left(\theta_1 - \theta_2\right) \\ & + 2 l_1\left(l_4 - d_4\right)\dot{\theta}_1\dot{\theta}_4 \cos\left(\theta_1 + \theta_4\right) \\ & + 2 l_2\left(l_4 - d_4\right)\dot{\theta}_2\dot{\theta}_4 \cos\left(\theta_2 - \theta_4\right)\}, \end{aligned} \tag{A3d}$$

and finally

$$\begin{aligned} \mathbf{v}_{c5} = {} & \begin{pmatrix} l_1 \cos\theta_1 \\ -l_1 \sin\theta_1 \end{pmatrix}\dot{\theta}_1 + \begin{pmatrix} l_2 \cos\theta_2 \\ -l_2 \sin\theta_2 \end{pmatrix}\dot{\theta}_2 + \begin{pmatrix} l_4 \cos\theta_4 \\ l_4 \sin\theta_4 \end{pmatrix}\dot{\theta}_4 \\ & + \begin{pmatrix} \left(l_5 - d_5\right)\cos\theta_5 \\ \left(l_5 - d_5\right)\sin\theta_5 \end{pmatrix}\dot{\theta}_5 \Longrightarrow \end{aligned}$$

$$\begin{aligned} K_5 = {} & \frac{1}{2}\left[I_5 + m_5\left(l_5 - d_5\right)^2\right]\left(\dot{\theta}_5\right)^2 \\ & + \frac{1}{2} m_5 \{ l_1^2\left(\dot{\theta}_1\right)^2 + l_2\left(\dot{\theta}_2\right)^2 + 2 l_1 l_2 \dot{\theta}_1\dot{\theta}_2 \cos\left(\theta_1 - \theta_2\right) \\ & + 2 l_1 l_4 \dot{\theta}_1\dot{\theta}_4 \cos\left(\theta_1 + \theta_4\right) + 2 l_2 l_4 \dot{\theta}_2\dot{\theta}_4 \cos\left(\theta_2 + \theta_4\right) \\ & + 2 l_1\left(l_5 - d_5\right)\dot{\theta}_1\dot{\theta}_5 \cos\left(\theta_1 + \theta_5\right) + 2 l_2\left(l_5 - d_5\right)\dot{\theta}_2\dot{\theta}_5 \cos\left(\theta_2 + \theta_5\right) \\ & + 2 l_4\left(l_5 - d_5\right)\dot{\theta}_4\dot{\theta}_5 \cos\left(\theta_4 - \theta_5\right)\}. \end{aligned} \tag{A3e}$$

Thus the total kinetic energy of the biped is

$$K = \sum_{i=1}^{5} K_i$$

from which one obtains:

$$\begin{aligned}
\frac{\mathrm{d}}{\mathrm{d}t}\left\{\frac{\partial K}{\partial \dot{\theta}_1}\right\} = \frac{\mathrm{d}}{\mathrm{d}t}\{&(I_1 + m_1 d_1^2)\dot{\theta}_1 \\
&+ (m_2 l_1^2)\dot{\theta}_1 + (m_2 d_2 l_1)\dot{\theta}_2 \cos(\theta_1 - \theta_2) \\
&+ (m_3 l_1^2)\dot{\theta}_1 + (m_3 l_1 l_2)\dot{\theta}_2 \cos(\theta_1 - \theta_2) \\
&+ (m_3 l_1 d_3)\dot{\theta}_3 \cos(\theta_1 - \theta_3) \\
&+ (m_4 l_1^2)\dot{\theta}_1 + (m_4 l_1 l_2)\dot{\theta}_2 \cos(\theta_1 - \theta_2) \\
&+ m_4 l_1 (l_4 - d_4)\dot{\theta}_4 \cos(\theta_1 + \theta_4) \\
&+ (m_5 l_1^2)\dot{\theta}_1 + (m_5 l_1 l_2)\dot{\theta}_2 \cos(\theta_1 - \theta_2) \\
&+ m_5 l_1 l_4 \dot{\theta}_4 \cos(\theta_1 + \theta_4) \\
&+ m_5 l_1 (l_5 - d_5)\dot{\theta}_5 \cos(\theta_1 + \theta_5)\} \\
= [&I_1 + m_1 d_1^2 + (m_2 + m_3 + m_4 + m_5) l_1^2]\ddot{\theta}_1 \\
&+ [m_2 d_2 l_1 + (m_3 + m_4 + m_5) l_1 l_2]\ddot{\theta}_2 \cos(\theta_1 - \theta_2) \\
&+ [m_3 l_1 d_3]\ddot{\theta}_3 \cos(\theta_1 - \theta_3) \\
&+ [m_4 l_1 (l_4 - d_4) + m_5 l_1 l_4]\ddot{\theta}_4 \cos(\theta_1 + \theta_4) \\
&+ [m_5 l_1 (l_5 - d_5)]\ddot{\theta}_5 \cos(\theta_1 + \theta_5) \\
&- [m_2 d_2 l_1 + (m_3 + m_4 + m_5) l_1 l_2]\dot{\theta}_1 \dot{\theta}_2 \sin(\theta_1 - \theta_2) \\
&+ [m_2 d_2 l_1 + (m_3 + m_4 + m_5) l_1 l_2](\dot{\theta}_2)^2 \sin(\theta_1 - \theta_2) \\
&- [m_3 l_1 d_3]\dot{\theta}_1 \dot{\theta}_3 \sin(\theta_1 - \theta_3) \\
&+ [m_3 l_1 d_3](\dot{\theta}_3)^2 \sin(\theta_1 - \theta_3) \\
&- [m_4 l_1 (l_4 - d_4) + m_5 l_1 l_4]\dot{\theta}_1 \dot{\theta}_4 \sin(\theta_1 + \theta_4) \\
&- [m_4 l_1 (l_4 - d_4) + m_5 l_1 l_4](\dot{\theta}_4)^2 \sin(\theta_1 + \theta_4) \\
&- [m_5 l_1 (l_5 - d_5)]\dot{\theta}_1 \dot{\theta}_5 \sin(\theta_1 + \theta_5) \\
&- [m_5 l_1 (l_5 - d_5)](\dot{\theta}_5)^2 \sin(\theta_1 + \theta_5), \qquad \text{(A4a)}
\end{aligned}$$

$$\begin{aligned}
\frac{\mathrm{d}}{\mathrm{d}t}\left\{\frac{\partial K}{\partial \dot{\theta}_2}\right\} = &[I_2 + m_2 d_2^2 + (m_3 + m_4 + m_5) l_2^2]\ddot{\theta}_2 \\
&+ [m_2 l_1 d_2 + (m_3 + m_4 + m_5) l_1 l_2]\ddot{\theta}_1 \cos(\theta_1 - \theta_2)
\end{aligned}$$

$$\begin{aligned}
&+ [m_3 l_2 d_3]\ddot{\theta}_3 \cos(\theta_2 - \theta_3) \\
&+ [m_4 l_2 (l_4 - d_4) + m_5 l_2 l_4]\ddot{\theta}_4 \cos(\theta_2 + \theta_4) \\
&+ [m_5 l_2 (l_5 - d_5)]\ddot{\theta}_5 \cos(\theta_2 + \theta_5) \\
&- [m_2 l_1 d_2 + (m_3 + m_4 + m_5) l_1 l_2](\dot{\theta}_1)^2 \sin(\theta_1 - \theta_2) \\
&+ [m_2 l_1 d_2 + (m_3 + m_4 + m_5) l_1 l_2]\dot{\theta}_1 \dot{\theta}_2 \sin(\theta_1 - \theta_2) \\
&+ [m_3 l_2 d_3](\dot{\theta}_3)^2 \sin(\theta_2 - \theta_3) \\
&- [m_3 l_2 d_3]\dot{\theta}_2 \dot{\theta}_3 \sin(\theta_2 - \theta_3) \\
&- [m_4 l_2 (l_4 - d_4) + m_5 l_2 l_4](\dot{\theta}_4)^2 \sin(\theta_2 + \theta_4) \\
&- [m_4 l_2 (l_4 - d_4) + m_5 l_2 l_4]\dot{\theta}_2 \dot{\theta}_4 \sin(\theta_2 + \theta_4) \\
&- [m_5 l_2 (l_5 - d_5)](\dot{\theta}_5)^2 \sin(\theta_5 + \theta_5) \\
&- [m_5 l_2 (l_5 - d_5)]\dot{\theta}_2 \dot{\theta}_5 \sin(\theta_2 + \theta_5), \qquad \text{(A4b)}
\end{aligned}$$

$$\begin{aligned}
\frac{\mathrm{d}}{\mathrm{d}t}\left\{\frac{\partial K}{\partial \dot{\theta}_3}\right\} = &[I_3 + m_3 d_3^2]\ddot{\theta}_3 \\
&+ [m_3 l_1 d_3]\ddot{\theta}_1 \cos(\theta_1 - \theta_3) \\
&+ [m_3 l_2 d_3]\ddot{\theta}_2 \cos(\theta_2 - \theta_3) \\
&- [m_3 l_1 d_3](\dot{\theta}_1)^2 \sin(\theta_1 - \theta_3) \\
&+ [m_3 l_1 d_3]\dot{\theta}_1 \dot{\theta}_3 \sin(\theta_1 - \theta_3) \\
&- [m_3 l_2 d_3](\dot{\theta}_2)^2 \sin(\theta_2 - \theta_3) \\
&+ [m_3 l_2 d_3]\dot{\theta}_2 \dot{\theta}_3 \sin(\theta_2 - \theta_3), \qquad \text{(A4c)}
\end{aligned}$$

$$\begin{aligned}
\frac{\mathrm{d}}{\mathrm{d}t}\left\{\frac{\partial K}{\partial \dot{\theta}_4}\right\} = &\left[I_4 + m_4 (l_4 - d_4)^2 + m_5 l_4^2\right]\ddot{\theta}_4 \\
&+ [m_4 l_1 (l_4 - d_4) + m_5 l_1 l_4]\ddot{\theta}_1 \cos(\theta_1 + \theta_4) \\
&+ [m_4 l_2 (l_4 - d_4) + m_5 l_2 l_4]\ddot{\theta}_2 \cos(\theta_2 + \theta_4) \\
&+ [m_5 l_4 (l_5 - d_5)]\ddot{\theta}_5 \cos(\theta_4 - \theta_5) \\
&- [m_4 l_1 (l_4 - d_4) + m_5 l_1 l_4](\dot{\theta}_1)^2 \sin(\theta_1 + \theta_4) \\
&- [m_4 l_1 (l_4 - d_4) + m_5 l_1 l_4]\dot{\theta}_1 \dot{\theta}_4 \sin(\theta_1 + \theta_4) \\
&- [m_4 l_2 (l_4 - d_4) + m_5 l_2 l_4](\dot{\theta}_2)^2 \sin(\theta_2 + \theta_4) \\
&- [m_4 l_2 (l_4 - d_4) + m_5 l_2 l_4]\dot{\theta}_2 \dot{\theta}_4 \sin(\theta_2 + \theta_4)
\end{aligned}$$

$$+ [m_5 l_4 (l_5 - d_5)] (\dot{\theta}_5)^2 \sin(\theta_4 - \theta_5)$$
$$- [m_5 l_4 (l_5 - d_5)] \dot{\theta}_4 \dot{\theta}_5 \sin(\theta_4 - \theta_5), \tag{A4d}$$

$$\frac{\mathrm{d}}{\mathrm{d}t}\left\{\frac{\partial K}{\partial \dot{\theta}_5}\right\} = \left[I_5 + m_5 (l_5 - d_5)^2\right] \ddot{\theta}_5$$
$$+ [m_5 l_1 (l_5 - d_5)] \ddot{\theta}_1 \cos(\theta_1 + \theta_5)$$
$$+ [m_5 l_2 (l_5 - d_5)] \ddot{\theta}_2 \cos(\theta_2 + \theta_5)$$
$$+ [m_5 l_4 (l_5 - d_5)] \ddot{\theta}_4 \cos(\theta_4 - \theta_5)$$
$$- [m_5 l_1 (l_5 - d_5)] (\dot{\theta}_1)^2 \sin(\theta_1 + \theta_5)$$
$$- [m_5 l_1 (l_5 - d_5)] \dot{\theta}_1 \dot{\theta}_5 \sin(\theta_1 + \theta_5)$$
$$- [m_5 l_2 (l_5 - d_5)] (\dot{\theta}_2)^2 \sin(\theta_2 + \theta_5)$$
$$- [m_5 l_2 (l_5 - d_5)] \dot{\theta}_2 \dot{\theta}_5 \sin(\theta_2 + \theta_5)$$
$$- [m_5 l_4 (l_5 - d_5)] (\dot{\theta}_4)^2 \sin(\theta_4 - \theta_5)$$
$$+ [m_5 l_4 (l_5 - d_5)] \dot{\theta}_4 \dot{\theta}_5 \sin(\theta_4 - \theta_5). \tag{A4e}$$

Also

$$\frac{\partial K}{\partial \theta_1} = -(m_2 d_2 l_1) \dot{\theta}_1 \dot{\theta}_2 \sin(\theta_1 - \theta_2)$$
$$- [(m_3 + m_4 + m_5) l_1 l_2] \dot{\theta}_1 \dot{\theta}_2 \sin(\theta_1 - \theta_2)$$
$$- [m_3 l_1 d_3] \dot{\theta}_1 \dot{\theta}_3 \sin(\theta_1 - \theta_3)$$
$$- [m_4 l_1 (l_4 - d_4) + m_5 l_1 l_4] \dot{\theta}_1 \dot{\theta}_4 \sin(\theta_1 + \theta_4)$$
$$- [m_5 l_1 (l_5 - d_5)] \dot{\theta}_1 \dot{\theta}_5 \sin(\theta_1 + \theta_5), \tag{A5a}$$

$$\frac{\partial K}{\partial \theta_2} = (m_2 d_2 l_1) \dot{\theta}_1 \dot{\theta}_2 \sin(\theta_1 - \theta_2)$$
$$+ [(m_3 + m_4 + m_5) l_1 l_2] \dot{\theta}_1 \dot{\theta}_2 \sin(\theta_1 - \theta_2)$$
$$- [m_3 l_2 d_3] \dot{\theta}_2 \dot{\theta}_3 \sin(\theta_2 - \theta_3)$$
$$- [m_4 l_2 (l_4 - d_4) + m_5 l_2 l_4] \dot{\theta}_2 \dot{\theta}_4 \sin(\theta_2 + \theta_4)$$
$$- [m_5 l_2 (l_5 - d_5)] \dot{\theta}_2 \dot{\theta}_5 \sin(\theta_2 + \theta_5), \tag{A5b}$$

$$\frac{\partial K}{\partial \theta_3} = [m_3 l_1 d_3] \dot{\theta}_1 \dot{\theta}_3 \sin(\theta_1 - \theta_3)$$
$$+ [m_3 l_2 d_3] \dot{\theta}_2 \dot{\theta}_3 \sin(\theta_2 - \theta_3), \tag{A5c}$$

$$\frac{\partial K}{\partial \theta_4} = -[m_4 l_1 (l_4 - d_4) + m_5 l_1 l_4] \dot{\theta}_1 \dot{\theta}_4 \sin(\theta_1 + \theta_4)$$
$$- [m_4 l_2 (l_4 - d_4) + m_5 l_2 l_4] \dot{\theta}_2 \dot{\theta}_4 \sin(\theta_2 + \theta_4)$$
$$- [m_5 l_4 (l_5 - d_5)] \dot{\theta}_4 \dot{\theta}_5 \sin(\theta_4 - \theta_5), \tag{A5d}$$

$$\frac{\partial K}{\partial \theta_5} = -[m_5 l_1 (l_5 - d_5)] \dot{\theta}_1 \dot{\theta}_5 \sin(\theta_1 + \theta_5)$$
$$- [m_5 l_2 (l_5 - d_5)] \dot{\theta}_2 \dot{\theta}_5 \sin(\theta_2 + \theta_5)$$
$$+ [m_5 l_4 (l_5 - d_5)] \dot{\theta}_4 \dot{\theta}_5 \sin(\theta_4 - \theta_5). \tag{A5e}$$

Using (A2a–e), (A3a–e) and (A4a–e) in (A1) one obtains the desired model (5).

6.2. APPENDIX 2. Transformation of the biped model (5) to the model (12 a–c)

The generalized torques T_{qi} $(i = 0, 1, \ldots, 4)$ that correspond to the variables: $q_0 = \theta_1$, $q_1 = \theta_1 - \theta_2$, $q_2 = \theta_2 - \theta_3$, $q_3 = \theta_3 + \theta_4$ and $q_4 = \theta_4 - \theta_5$ are:

$$T_{q0} = 0, \qquad T_{qi} = \tau_i \qquad (i = 1, \ldots, 4), \tag{A6}$$

where τ_i are the actual driving torques of the four joints. The fact that $T_{q0} = 0$ indicates that the angle q_0 of the hypothetical joint 0 is not directly controlled by a driving torque.

The variables θ_i $(i = 1, 2, \ldots, 5)$ are expressed in terms of the q_i's $(i = 0, 1, \ldots, 4)$ as:

$$\left.\begin{aligned} \theta_1 &= q_0, \\ \theta_2 &= \theta_1 - q_1 = q_0 - q_1, \\ \theta_3 &= \theta_2 - q_2 = q_0 - q_1 - q_2, \\ \theta_4 &= q_3 - \theta_3 = -q_0 + q_1 + q_2 + q_3, \\ \theta_5 &= \theta_4 - q_4 = -q_0 + q_1 + q_2 + q_3 - q_4. \end{aligned}\right\} \tag{A7}$$

Thus, from the relation

$$T_{qi} = \sum_{j=1}^{5} T_{\theta_j} \frac{\partial q_j}{\partial q_i}, \qquad i = 0, \ldots, 5,$$

one obtains:

$$\left.\begin{aligned} T_{q0} &= T_{\theta 1} + T_{\theta 2} + T_{\theta 3} - T_{\theta 4} - T_{\theta 5}, \\ T_{q1} &= -T_{\theta 2} - T_{\theta 3} + T_{\theta 4} + T_{\theta 5}, \\ T_{q2} &= -T_{\theta 3} + T_{\theta 4} + T_{\theta 5}, \\ T_{q3} &= T_{\theta 4} + T_{\theta 5}, \\ T_{q4} &= -T_{\theta 5}. \end{aligned}\right\} \quad \text{(A8)}$$

Now, using (A6), (A7) and (A8) the biped model (5) is transformed as follows:

$$A_{11}\ddot{\theta}_1 + A_{12}\ddot{\theta}_2 + A_{13}\ddot{\theta}_3 + A_{14}\ddot{\theta}_4 + A_{15}\ddot{\theta}_5 + h_{q0} + G_{q0} = T_{q0} = 0 \quad \text{(A9a)}$$

where

$$\begin{aligned} A_{1j} &= D_{1j} + D_{2j} + D_{3j} - D_{4j} - D_{5j}, \qquad j = 1, \ldots, 5, \\ h_{q0} &= h_1 + h_2 + h_3 - h_4 - h_5, \\ G_{q0} &= G_1 + G_2 + G_3 - G_4 + G_5. \end{aligned}$$

$$A_{21}\ddot{\theta}_1 + A_{22}\ddot{\theta}_2 + A_{23}\ddot{\theta}_3 + A_{24}\ddot{\theta}_4 + A_{25}\ddot{\theta}_5 + h_{q1} + G_{q1} = T_{q1} = \tau_1 \quad \text{(A9b)}$$

where

$$\begin{aligned} A_{2j} &= -D_{2j} - D_{3j} + D_{4j} + D_{5j}, \qquad j = 1, \ldots, 5 \\ h_{q1} &= -h_2 - h_3 + h_4 + h_5, \qquad G_{q1} = -G_2 - G_3 + G_4 + G_5. \end{aligned}$$

$$A_{31}\ddot{\theta}_1 + A_{32}\ddot{\theta}_2 + A_{33}\ddot{\theta}_3 + A_{34}\ddot{\theta}_4 + A_{35}\ddot{\theta}_5 + h_{q2} + G_{q2} = T_{q2} = \tau_2 \quad \text{(A9c)}$$

where

$$\begin{aligned} A_{3j} &= -D_{3j} + D_{4j} + D_{5j}, \qquad j = 1, \ldots, 5, \\ h_{q2} &= -h_3 + h_4 + h_5, \qquad G_{q2} = -G_3 + G_4 + G_5. \end{aligned}$$

$$A_{41}\ddot{\theta}_1 + A_{42}\ddot{\theta}_2 + A_{43}\ddot{\theta}_3 + A_{44}\ddot{\theta}_4 + A_{45}\ddot{\theta}_5 + h_{q3} + G_{q3} = T_{q3} = \tau_3 \quad \text{(A9d)}$$

where

$$\begin{aligned} A_{4j} &= D_{4j} + D_{5j}, \qquad j = 1, \ldots, 5, \\ h_{q3} &= h_4 + h_5, \qquad G_{q3} = G_4 + G_5. \end{aligned}$$

$$A_{51}\ddot{\theta}_1 + A_{52}\ddot{\theta}_2 + A_{53}\ddot{\theta}_3 + A_{54}\ddot{\theta}_4 + A_{55}\ddot{\theta}_5 + h_{q4} + G_{q4} = T_{q4} = \tau_4 \quad \text{(A9e)}$$

where

$$\begin{aligned} A_{5j} &= -D_{5j}, \qquad j = 1, \ldots, 5, \\ h_{q4} &= -h_5, \qquad G_{q4} = -G_5. \end{aligned}$$

Finally, using the transformations (A7) one obtains the transformed biped dynamic model (12 a–c) as desired. It is easy to verify that the new inertia matrix $\mathbf{D}_a$ is symmetric, as expected.

6.3. APPENDIX 3. Derivation of the biped dynamic model (13)

The model (13) is again derived by applying the Langrange Equation (A1). The potential energy of the system in the air (Figure 3) is:

$$\begin{aligned} U = {} & m_1 g(y_b + d_1 \cos\theta_1) \\ & + m_2 g(y_b + l_1 \cos\theta_1 + d_2 \cos\theta_2) \\ & + m_3 g(y_b + l_1 \cos\theta_1 + l_2 \cos\theta_2 + d_3 \cos\theta_3) \\ & + m_4 g(y_b + l_1 \cos\theta_1 + l_2 \cos\theta_2 - (l_4 - d_4)\cos\theta_4) \\ & + m_5 g(y_b + l_1 \cos\theta_1 + l_2 \cos\theta_2 - l_4 \cos\theta_4 - (l_5 - d_5)\cos\theta_5). \end{aligned}$$

Therefore

$$\frac{\partial U}{\partial \theta_i} = G_i, \qquad i = 1, \ldots, 5, \quad \text{(A10)}$$

where the G_i's are as defined in (6), and

$$\begin{aligned} \frac{\partial U}{\partial x_b} &= 0, \\ \frac{\partial U}{\partial y_b} &= (m_1 + m_2 + m_3 + m_4 + m_5)\, g = m_{o\lambda} \cdot g. \end{aligned}$$

The kinetic energy of link i is given by

$$K_i = \frac{1}{2} m_i \mathbf{v}_{ci}^2 + \frac{1}{2} I_i (\dot{\theta}_i)^2 \qquad (i = 1, \ldots, 5),$$

where $\mathbf{v}_{ci}$ is the velocity of the center of mass of link i. Thus using the relations (A3) and the fact that the velocities $\mathbf{v}_{ci}$ for the model in the air are increased

by $(x_b, y_b)^T$ one obtains:

$$K_1 = \frac{1}{2}\left(I_1 + m_1 d_1^2\right)(\dot\theta_1)^2 + \frac{1}{2} m_1\Big[(\dot x_b)^2 + (\dot y_b)^2 + 2d_1\dot\theta_1(\dot x_b\cos\theta_1 - \dot y_b\sin\theta_1)\Big],$$

$$\mathbf{v}_{c2} = \begin{pmatrix}\dot x_b\\ \dot y_b\end{pmatrix} + \begin{pmatrix}\cos\theta_1\\ -\sin\theta_1\end{pmatrix} l_1\dot\theta_1 + \begin{pmatrix}\cos\theta_2\\ -\sin\theta_2\end{pmatrix} d_2\dot\theta_2 \Longrightarrow$$

$$K_2 = \frac{1}{2}\left(I_2 + m_2 d_2^2\right)(\dot\theta_2)^2 + \frac{1}{2} m_2\Big[(\dot x_b)^2 + (\dot y_b)^2 + l_1^2(\dot\theta_1)^2 + (2l_1 d_2)\dot\theta_1\dot\theta_2\cos(\theta_1 - \theta_2), + 2l_1\dot\theta_1(\dot x_b\cos\theta_1 - \dot y_b\sin\theta_1) + 2d_2\dot\theta_2(\dot x_b\cos\theta_2 - \dot y_b\sin\theta_2)\Big],$$

$$\mathbf{v}_{c3} = \begin{pmatrix}\dot x_b\\ \dot y_b\end{pmatrix} + \begin{pmatrix}\cos\theta_1\\ -\sin\theta_1\end{pmatrix} l_1\dot\theta_1 + \begin{pmatrix}\cos\theta_2\\ -\sin\theta_2\end{pmatrix} l_2\dot\theta_2 + \begin{pmatrix}\cos\theta_3\\ -\sin\theta_3\end{pmatrix} d_3\dot\theta_3 \Longrightarrow$$

$$K_3 = \frac{1}{2}\left(I_3 + m_3 d_3^2\right)(\dot\theta_3)^2 + \frac{1}{2} m_3\Big[l_1^2(\dot\theta_1)^2 + l_2^2(\dot\theta_2)^2 + 2l_1 l_2\dot\theta_1\dot\theta_2\cos(\theta_1 - \theta_2) + 2l_1 d_3\dot\theta_1\dot\theta_3\cos(\theta_1 - \theta_3) + 2l_2 d_3\dot\theta_2\dot\theta_3\cos(\theta_2 - \theta_3)\Big] + \frac{1}{2} m_3\Big[(\dot x_b)^2 + (\dot y_b)^2 + 2l_1\dot\theta_1(\dot x_b\cos\theta_1 - \dot y_b\sin\theta_1) + 2l_2\dot\theta_2(\dot x_b\cos\theta_2 - \dot y_b\sin\theta_2) + 2d_3\dot\theta_3(\dot x_b\cos\theta_3 - \dot y_b\sin\theta_3)\Big].$$

Similarly

$$K_4 = \frac{1}{2}\left[I_4 + m_4(l_4 - d_4)^2\right](\dot\theta_4)^2 + \frac{1}{2} m_4\Big[l_1^2(\dot\theta_1)^2 + l_2^2(\dot\theta_2)^2 + 2l_1 l_2\dot\theta_1\dot\theta_2\cos(\theta_1 - \theta_2) + 2l_1(l_4 - d_4)\dot\theta_1\dot\theta_4\cos(\theta_1 + \theta_4) + 2l_2(l_4 - d_4)\dot\theta_2\dot\theta_4\cos(\theta_2 + \theta_4)\Big] + \frac{1}{2} m_4\Big[(\dot x_b)^2 + (\dot y_b)^2 + 2l_1\dot\theta_1(\dot x_b\cos\theta_1 - \dot y_b\sin\theta_1) + 2l_2\dot\theta_2(\dot x_b\cos\theta_2 - \dot y_b\sin\theta_2) + 2(l_4 - d_4)\dot\theta_4(\dot x_b\cos\theta_4 + \dot y_b\sin\theta_4)\Big],$$

$$K_5 = \frac{1}{2}\left[I_5 + m_5(l_5 - d_5)^2\right](\dot\theta_5)^2 + \frac{1}{2} m_5\Big[l_1^2(\dot\theta_1)^2 + l_2^2(\dot\theta_2)^2 + l_4^2(\dot\theta_4)^2 + 2l_1 l_2\dot\theta_1\dot\theta_2\cos(\theta_1 - \theta_2) + 2l_1 l_4\dot\theta_1\dot\theta_4\cos(\theta_1 + \theta_4) + 2l_2 l_4\dot\theta_2\dot\theta_4\cos(\theta_2 + \theta_4) + 2l_1(l_5 - d_5)\dot\theta_1\dot\theta_5\cos(\theta_1 + \theta_5) + 2l_2(l_5 - d_5)\dot\theta_2\dot\theta_5\cos(\theta_2 + \theta_5) + 2l_4(l_5 - d_5)\dot\theta_4\dot\theta_5\cos(\theta_4 - \theta_5)\Big] + \frac{1}{2} m_5\Big[(\dot x_b)^2 + (\dot y_b)^2 + 2l_1\dot\theta_1(\dot x_b\cos\theta_1 - \dot y_b\sin\theta_1) + 2l_2\dot\theta_2(\dot x_b\cos\theta_2 - \dot y_b\sin\theta_2) + 2l_4\dot\theta_4(\dot x_b\cos\theta_4 + \dot y_b\sin\theta_4)\Big] + 2(l_5 - d_5)\dot\theta_5(\dot x_b\cos\theta_5 + \dot y_b\sin\theta_5)\Big]. \tag{A11}$$

We thus obtain:

$$\frac{\mathrm{d}}{\mathrm{d}t}\left\{\frac{\partial K}{\partial\dot\theta_1}\right\} = \cdots + m_1 d_1(\ddot x_b\cos\theta_1 - \ddot y_b\sin\theta_1 - \dot x_b\dot\theta_1\sin\theta_1 - \dot y_b\dot\theta_1\cos\theta_1) + (m_2 + m_3 + m_4 + m_5) \times l_1(\ddot x_b\cos\theta_1 - \ddot y_b\sin\theta_1 - \dot x_b\dot\theta_1\sin\theta_1 - \dot y_b\dot\theta_1\cos\theta_1),$$

$$\frac{\mathrm{d}}{\mathrm{d}t}\left\{\frac{\partial K}{\partial\dot\theta_2}\right\} = \cdots + m_2 d_2(\ddot x_b\cos\theta_2 - \ddot y_b\sin\theta_2 - \dot x_b\dot\theta_2\sin\theta_2 - \dot y_b\dot\theta_2\cos\theta_2) + (m_3 + m_4 + m_5) \times l_2(\ddot x_b\cos\theta_2 - \ddot y_b\sin\theta_2 - \dot x_b\dot\theta_2\sin\theta_2 - \dot y_b\dot\theta_2\cos\theta_2),$$

$$\frac{\mathrm{d}}{\mathrm{d}t}\left\{\frac{\partial K}{\partial\dot\theta_3}\right\} = \cdots + (m_3 d_3) \times (\ddot x_b\cos\theta_3 - \ddot y_b\sin\theta_3 - \dot x_b\dot\theta_3\sin\theta_3 - \dot y_b\dot\theta_3\cos\theta_3),$$

$$\frac{\mathrm{d}}{\mathrm{d}t}\left\{\frac{\partial K}{\partial\dot\theta_4}\right\} = \cdots + \left[m_4(l_4 - d_4) + m_5 l_4\right] \times (\ddot x_b\cos\theta_4 + \ddot y_b\sin\theta_4 - \dot x_b\dot\theta_4\sin\theta_4 + \dot y_b\dot\theta_4\cos\theta_4),$$

$$\frac{\mathrm{d}}{\mathrm{d}t}\left\{\frac{\partial K}{\partial \dot{\theta}_5}\right\} = \cdots + \left[m_5(l_5 - d_5)\right] \times \left(\ddot{x}_b \cos\theta_5 + \ddot{y}_b \sin\theta_5 - \dot{x}_b\dot{\theta}_5 \sin\theta_5 + \dot{y}_b\dot{\theta}_5 \cos\theta_5\right),$$

$$\frac{\partial K}{\partial \theta_1} = \cdots + m_1 d_1 \dot{\theta}_1\left(-\dot{x}_b \sin\theta_1 - \dot{y}_b \cos\theta_1\right),$$

$$\frac{\partial K}{\partial \theta_2} = \cdots + m_2 d_2 \dot{\theta}_2\left(-\dot{x}_b \sin\theta_2 - \dot{y}_b \cos\theta_2\right),$$

$$\frac{\partial K}{\partial \theta_3} = \cdots + m_3 d_3 \dot{\theta}_3\left(-\dot{x}_b \sin\theta_3 - \dot{y}_b \cos\theta_3\right),$$

$$\frac{\partial K}{\partial \theta_4} = \cdots + \left[m_4(l_4 - d_4) + m_5 l_4\right]\dot{\theta}_4\left(-\dot{x}_b \sin\theta_4 + \dot{y}_b \cos\theta_4\right),$$

$$\frac{\partial K}{\partial \theta_5} = \cdots + \left[m_5(l_5 - d_5)\right]\dot{\theta}_5\left(-\dot{x}_b \sin\theta_5 + \dot{y}_b \cos\theta_5\right), \tag{A12}$$

where the three dots '$\cdots$' in the above relations represent the corresponding right hand sides of (A4a–e) and (A5a–e). Also, the following relations hold:

$$\begin{aligned}\frac{\mathrm{d}}{\mathrm{d}t}\left\{\frac{\partial K}{\partial \dot{x}_b}\right\} &= (m_1 + m_2 + m_3 + m_4 + m_5)\ddot{x}_b \\ &+ m_1 d_1 \ddot{\theta}_1 \cos\theta_1 - m_1 d_1 (\dot{\theta}_1)^2 \sin\theta_1 \\ &+ (m_2 + m_3 + m_4 + m_5) l_1 \ddot{\theta}_1 \cos\theta_1 \\ &- (m_2 + m_3 + m_4 + m_5) l_1 (\dot{\theta}_1)^2 \sin\theta_1 \\ &+ \left[m_2 d_2 + (m_3 + m_4 + m_5) l_2\right]\ddot{\theta}_2 \cos\theta_2 \\ &- \left[m_2 d_2 + (m_3 + m_4 + m_5) l_2\right](\dot{\theta}_2)^2 \sin\theta_2 \\ &+ (m_3 d_3)\ddot{\theta}_3 \cos\theta_3 - (m_3 d_3)(\dot{\theta}_3)^2 \sin\theta_3 \\ &+ \left[m_4(l_4 - d_4) + m_5 l_4\right]\ddot{\theta}_4 \cos\theta_4 \\ &- \left[m_4(l_4 - d_4) + m_5 l_4\right](\dot{\theta}_4)^2 \sin\theta_4 \\ &+ \left[m_5(l_5 - d_5)\right]\ddot{\theta}_5 \cos\theta_5 - \left[m_5(l_5 - d_5)\right](\dot{\theta}_5)^2 \sin\theta_5,\end{aligned}$$

$$\begin{aligned}\frac{\mathrm{d}}{\mathrm{d}t}\left\{\frac{\partial K}{\partial \dot{y}_b}\right\} &= (m_1 + m_2 + m_3 + m_4 + m_5)\ddot{y}_b \\ &- m_1 d_1 \ddot{\theta}_1 \sin\theta_1 - m_1 d_1 (\dot{\theta}_1)^2 \cos\theta_1 \\ &- (m_2 + m_3 + m_4 + m_5) l_1 \ddot{\theta}_1 \sin\theta_1 \\ &- (m_2 + m_3 + m_4 + m_5) l_1 (\dot{\theta}_1)^2 \cos\theta_1 \\ &- \left[m_2 d_2 + (m_3 + m_4 + m_5) l_2\right]\ddot{\theta}_2 \sin\theta_2 \\ &- \left[m_2 d_2 + (m_3 + m_4 + m_5) l_2\right](\dot{\theta}_2)^2 \cos\theta_2 \\ &- (m_3 d_3)\ddot{\theta}_3 \sin\theta_3 - (m_3 d_3)(\dot{\theta}_3)^2 \cos\theta_3 \\ &+ \left[m_4(l_4 - d_4) + m_5 l_4\right]\ddot{\theta}_4 \sin\theta_4 \\ &+ \left[m_4(l_4 - d_4) + m_5 l_4\right](\dot{\theta}_4)^2 \cos\theta_4 \\ &+ \left[m_5(l_5 - d_5)\right]\ddot{\theta}_5 \sin\theta_5 + \left[m_5(l_5 - d_5)\right](\dot{\theta}_5)^2 \cos\theta_5,\end{aligned}$$

$$\frac{\partial K}{\partial x_b} = 0,$$

$$\frac{\partial K}{\partial y_b} = 0. \tag{A13}$$

Using (A10) through (A13) in the Lagrange Equation (A1) gives the desired biped model (13).

6.4. APPENDIX 4. Derivation of the collision formula (18)

The impact of a robot with its environment is a common phenomenon in all robotic systems. Industrial robots have to perform some desired tasks which require the robot to come in contact with the object under processing and exert upon it a suitable force. The impact phenomenon occurs exactly at the moment when the robotic end effector touches the object. On the other hand the impact phenomenon in legged robots takes place each time the robot exchanges the leg(s) of support.

The impact with the environment implies a sharp change of the joint velocities [17]. It is therefore required to compute each time the new joint velocities just after each collision. Actually at the moment when the robot comes into contact with the environment, a geometric constraint is enforced to the system motion.

Let $\mathbf{x}_e$ be the instantaneous position/orientation of the robotic end which comes into contact with the environment, expressed with respect to the world coordinate

(inertia reference) system. Then we have

$$\mathbf{x}_e = \mathbf{x}_e(\boldsymbol{\theta}), \tag{A14}$$

where $\boldsymbol{\theta} = [\theta_1, \ldots, \theta_n]^T$ is the vector of generalized coordinates of the system. If $\mathbf{x}_s$ is the contact point, the collision occurs when

$$\mathbf{x}_e(\boldsymbol{\theta}) = \mathbf{x}_s. \tag{A15}$$

Equation (A15) represents an external constraint to the robot motion. Every external constraint implies the introduction of a generalized constraint force $\mathbf{F}_\delta$ in the system dynamic model, where

$$\mathbf{F}_\delta = \left[\frac{\partial \mathbf{x}_e}{\partial \underline{\theta}}\right]^T \underline{\lambda} = \mathbf{J}^T \underline{\lambda}, \tag{A16}$$

where $\mathbf{J}$ is the Jacobian and $\underline{\lambda}$ is a suitable column vector of Lagrange multipliers.

In this way, if the robotic dynamic model before the collision is (see Equation (5)):

$$\mathbf{D}(\theta)\ddot{\theta} + \mathbf{h}(\theta, \dot{\theta}) + \mathbf{G}(\theta) = \mathbf{T}_\theta \tag{A17}$$

then just after the collision becomes

$$\mathbf{D}(\theta)\ddot{\theta} + \mathbf{h}(\theta, \dot{\theta}) + \mathbf{G}(\theta) = \mathbf{T}_\theta + \mathbf{F}_\delta. \tag{A18}$$

During the infinitesimal duration of the collision the joint positions remain unchanged, since the joint velocities are finite and their integral over an infinitesimal time interval is zero. Integrating therefore (A18) over the infinitesimal interval $[t_0,\ t_0 + \Delta t]$ one obtains (t_0 is the instant of collision):

$$\begin{aligned} &\lim_{\Delta t \to 0} \int_{t_0}^{t_0+\Delta t} \mathbf{D}(\theta)\ddot{\theta}\,\mathrm{d}t + \lim_{\Delta t \to 0} \int_{t_0}^{t_0+\Delta t} \left[\mathbf{h}(\theta, \dot{\theta}) + \mathbf{G}(\theta) - \mathbf{T}_\theta\right]\mathrm{d}t \\ &\quad = \lim_{\Delta t \to 0} \int_{t_0}^{t_0+\Delta t} \mathbf{F}_\delta \cdot \mathrm{d}t. \end{aligned} \tag{A19}$$

The second term on the left hand side of (A19) goes to zero as $\Delta t \to 0$, and so (A19) reduces to

$$\mathbf{D}(\theta)\Delta\dot{\theta} = \boldsymbol{\Omega}_\delta, \tag{A20}$$

$$\Delta\dot{\theta} = \dot{\theta}(t_0 + \Delta t) - \dot{\theta}(t_0), \tag{A21a}$$

$$\boldsymbol{\Omega}_\delta = \int_{t_0}^{t_0+\Delta t} \mathbf{F}_\delta \cdot \mathrm{d}t \qquad \text{(a finite value)}. \tag{A21b}$$

Equation (A20) constitutes an expression of the theorem of conservation of momentum and allows the computation of $\Delta\dot{\theta}$ if $\boldsymbol{\Omega}_\delta$ is known. But in actual practice $\boldsymbol{\Omega}_\delta$ is not in general known. However, the relative velocity $\Delta\dot{\mathbf{x}}_e = \dot{\mathbf{x}}_e(t_0 + \Delta t) - \dot{\mathbf{x}}_e(t_0)$ between the contact points of the robot and the environment can be measured and used for the computation of $\Delta\underline{\dot{\theta}}$. To find the relation between $\Delta\dot{\mathbf{x}}_e$ and $\Delta\dot{\theta}$ we start from $\dot{\mathbf{x}}_e = \mathbf{J}\dot{\theta}$ and obtain

$$\dot{\mathbf{x}}_e - \dot{\mathbf{x}}_s = \mathbf{J}\dot{\theta} - \dot{\mathbf{x}}_s. \tag{A22}$$

Now, if all objects with which the robot comes into contact are not moving, (A22) gives

$$\mathbf{J}\left[\dot{\theta}(t_0 + \Delta t) - \dot{\theta}(t_0)\right] = \dot{\mathbf{x}}_e(t_0 + \Delta t) - \dot{\mathbf{x}}(t_0),$$

$$\text{i.e.} \qquad \mathbf{J}\Delta\dot{\theta} = \Delta\dot{\mathbf{x}}_e. \tag{A23}$$

Therefore, using (A16), (A20) and (A21b) in (A23) one obtains

$$\boldsymbol{\Omega}_\delta = \mathbf{J}^T \int_{t_0}^{t_0+\Delta t} \lambda \mathrm{d}t \qquad \text{and}$$

$$\mathbf{J}\Delta\dot{\theta} = \mathbf{J}\left[\mathbf{D}^{-1}(\theta) \cdot \underline{\mathbf{J}}^T \cdot \int_{t_0}^{t_0+\Delta t} \lambda \mathrm{d}t\right] = \Delta\dot{\mathbf{x}}_e.$$

Hence

$$\int_{t_0}^{t_0+\Delta t} \lambda \mathrm{d}t = \left[\mathbf{J}\mathbf{D}^{-1}\mathbf{J}^T\right]^{-1}\Delta\dot{\mathbf{x}}_e$$

or

$$\boldsymbol{\Omega}_\delta = \mathbf{J}^T\left(\mathbf{J}\mathbf{D}^{-1}\mathbf{J}^T\right)\Delta\dot{\mathbf{x}}_e. \tag{A24}$$

Equation (A24) allows the computation of $\boldsymbol{\Omega}_\delta$ by using the measured quantity $\Delta\dot{\mathbf{x}}_e$. Introducing (A24) into (A20) one obtains

$$\Delta\dot{\theta} = \mathbf{D}^{-1}\mathbf{J}^T\left(\mathbf{J}\mathbf{D}^{-1}\mathbf{J}^T\right)^{-1}\Delta\dot{\mathbf{x}}_e, \tag{A25}$$

i.e. the desired Equation (18).

Acknowledgement

This work was partially carried out under a visiting exchange grant of the AI Laboratory of MIT. S. Tzafestas expresses his thanks for this opportunity.

References

1. Raibert, M.: *Legged Robots that Balance*, MIT Press, Cambridge, MA, 1986.
2. Chow, C. K. and Jacobson: Further studies of human locomotion: Postural stability and control, *Math. Biosci.* **15** (1972), 93–108.
3. Hemami, H., Wil, C. and Goliday, G. L.: The inverted pendulum and biped stability, *Math. Biosci.* **34** (1977), 95–110.
4. Hemami, H. and Katbab, A.: Constrained inverted pendulum model for evaluating upright postural stability, *ASME J. Dyn. Syst. Meas. Contr.* **104** (1982), 343–349.
5. Mochon, S.: A mathematical model of human walking, *Lectures on Mathematics in Life Sciences*, Vol. 14, Amer. Math. Soc., 1981.
6. Hemami, H., Zheng, Y. F. and Hines, M. J.: Initiation of walk and tiptoe of a planar nine-link biped, *Math. Biosci.* **61** (1982), 163–189.
7. Miura, H. and Shinoyama, I.: Dynamic walk of a biped, *Intl. J. Robotics Res.* **3**(2) (1984).
8. Furusho, J. and Masubuchi, M.: Control of a dynamic biped locomotion system for steady walking, *ASME J. Dyn. Syst. Meas. Contr.* **108** (1986), 111–118.
9. Furusho, J. and Masubuchi, M.: A theoretically motivated reduced-order model for the control of dynamic biped locomotion, *ASME J. Dyn. Syst. Meas. Contr.* **109** (1987), 155–163.
10. Yamada, M., Furusho, J. and Sano, A.: Dynamic control of walking robot with kick-action, *Proc. 1985 Intl. Conf. on Advanced Robotics* (*ICAR'85*), pp. 405–412, Tokyo (1985).
11. Sano, A. and Furusho, J.: 3D steady walking robot with kick-action, *Proc. 1988 USA-Japan Symp. on Flexible Automation*, Vol. II, Minneapolis, July 1988.
12. Mita, T., Yamguchi, T., Kashiwase, T. and Kawase, T.: Realization of a high speed biped using modern control theory, *Int. J. Control* **40** (1984), 107–119.
13. Takanishi, A., Egusa, Y., Tochizawa, M., Takeya, T. and Kato, I.: Realization of dynamic biped walking stabilized with trunk motion, *Proc. Rob. Manuf. Syst.'88*, September 1988.
14. Slotine, J. J.: The robust control of robot manipulators, *Int. J. Robotics Res.* **4**(2) (1985).
15. Slotine, J. J. and Spong, M. W.: Robust robot control with bounded input torques, *Int. J. Robotics Res.* **2**(4) (1985).
16. Slotine, J. J. and Li, W.: *Applied Nonlinear Control*, Prentice Hall (1991).
17. Zheng, Y. F. and Hemami, H.: Mathematical modeling of a robot collision with its environment, *Int. J. Robotics Res.* **2**(3) (1985), 289–307.
18. Hemami, H. and Zheng, Y. F.: Dynamics and control of motion on the ground and in the air with application to biped robots, *J. Robotic Systems* **1**(1) (1984), 101–116.
19. Walker, M. W. and Orin, D.: Efficient dynamic computer simulation of robot mechanisms, *ASME J. Dyn. Syst. Meas. Control* **104** (1982), 205–211.
20. Luh, J. Y. S., Walker, M. W. and Paul, R. P. C.: On-line computational scheme for mechanical manipulators, *ASME J. Dyn. Syst. Meas. Control* **102** (1980), 69–76.
21. Zheng, Y.-F.: The study of a nine link biped model with two feet, *M.Sc. Thesis*, The Ohio State University (1980).

22. Sias, F. R. Jr. and Zheng, Y.- F.: How many degrees-of-freedom does a biped need? *Proc. IEEE Intl. Workshop on Intelligent Robots and Systems* (*IROS'90*), pp. 297–302 (1990).
23. Tzafestas, S. G., Dritsas, L. and Kanellakopoulos, J.: Robust robot control: A comparison of three techniques through simulation, in P. Breedverld et al. (eds), *Modeling and Simulation of Systems*, J. C. Baltzer Co., 1989, pp. 255–260.
24. Tzafestas, S. G.: Adaptive, robust and rule-based control of robotic manipulators, in S. G. Tzafestas (ed), *Intelligent Robotics Systems*, Marcel Dekker, 1991, pp. 313–419.
25. Jaworska, I. and Tzafestas, S.: Robust stability analysis of robot control systems, *Robotics and Autonomous Systems* **17** (1991), 285–290.
26. Tzafestas, S. G.: Task grouping and scheduling for parallel processing, in T. Ono and F. Kozin (eds), *Systems and Control–Topics in Theory and Applications*, MITA Press, 1991, pp. 401–419.